

Annual Review of Control, Robotics, and Autonomous Systems

Spacecraft-Mounted Robotics

Panagiotis Tsiotras, Matthew King-Smith, and Lorenzo Ticozzi

School of Aerospace Engineering, Georgia Institute of Technology, Atlanta, Georgia, USA; email: tsiotras@gatech.edu, mking-smith@gatech.edu, lorenzo@gatech.edu

ANNUAL CONNECT

www.annualreviews.org

- Download figures
- Navigate cited references
- · Keyword search
- · Explore related articles
- Share via email or social media

Annu. Rev. Control Robot. Auton. Syst. 2023. 6:335–62

First published as a Review in Advance on October 7, 2022

The Annual Review of Control, Robotics, and Autonomous Systems is online at control annual reviews.org

https://doi.org/10.1146/annurev-control-062122-082114

Copyright © 2023 by the author(s). This work is licensed under a Creative Commons Attribution 4.0 International License, which permits unrestricted use, distribution, and reproduction in any medium, provided the original author and source are credited. See credit lines of images or other third-party material in this article for license information.

Keywords

robotics, manipulators, in-orbit servicing, control, trajectory tracking, dual quaternions, dynamics, kinematics

Abstract

Space-mounted robotics is becoming increasingly mainstream for many space missions. The aim of this article is threefold: first, to give a broad and quick overview of the importance of spacecraft-mounted robotics for future in-orbit servicing missions; second, to review the basic current approaches for modeling and control of spacecraft-mounted robotic systems; and third, to introduce some new developments in terms of modeling and control of spacecraft-mounted robotic manipulators using the language of hypercomplex numbers (dual quaternions). Some outstanding research questions and potential future directions in the field are also discussed.



1. INTRODUCTION

Recent years have witnessed an exploding demand for space-based services, leading to a steady increase in the number of operational satellites orbiting Earth for commercial, scientific, or military purposes (1). In fact, environmental, economic, and strategic considerations support the claim that the future of a space infrastructure will depend on the ability to perform on-orbit servicing, encompassing a broad array of in-space operations, such as inspection, berthing, refueling, repair, assembly, and so on. It is certain that these operations will be carried out with the help of novel autonomous or semiautonomous robotic systems.

Space robotics is, without a doubt, a major factor that can help enormously in transitioning to routine space operations in environments that are harsh and dangerous for humans. Although, in general, space robotics is a large field, encompassing autonomous satellites and spacecraft, planetary rovers, and orbiting spacecraft equipped with articulated mechanisms, in this article we use the term space robotics to refer primarily to the last. Our objective is therefore to provide a brief overview of the (large) literature of spacecraft-mounted manipulator systems and, in particular, to highlight their envisioned utilization for future servicing missions in orbit.

The article is organized in roughly three distinct parts. In the first part, we provide a broad overview of the importance of spacecraft-mounted robotic systems (SMRSs) for future in-orbit servicing missions. In the second part, we review the current approaches for modeling and control of SMRSs. The third part introduces some new developments in terms of modeling and control of SMRSs using the language of hypercomplex numbers (i.e., dual quaternions). This mathematical formalism offers several advantages compared with more traditional approaches, stemming primarily from the resulting compact representation of the equations of motion and the ability to provide a unifying framework that encompasses the combined translational and rotational motions of the SMRSs without any simplifying (e.g., artificial decoupling) assumptions. Our hope is that this article will provide the reader with a better appreciation of both the challenges and the tremendous opportunities offered by space robotic missions.

1.1. Robotics as an Enabler of Space Servicing Missions

Access to space has enabled a wide range of commercial, scientific, and military activities that are only bound to continue. From space-based experimental laboratories, such as the International Space Station (ISS), to missile-tracking defense networks of satellites, to GPS-enabling geostationary satellites that aid our daily commutes, satellites provide valuable services to their operators, the scientific community, and society as a whole.

Even though launch costs are likely to decrease with the advent of reusable first-stage rockets, the wider use of commercial off-the-shelf components, and the miniaturization of electronics, sensors, and other equipment, access to space remains expensive and is expected to be so at least for the foreseeable future. It is not surprising, therefore, that there has been much recent interest in the possibility of servicing and repairing space assets in orbit. The 2010 NASA On-Orbit Satellite Servicing Study (2) highlighted how an evolution in the paradigm of space operations through robotics-enabled on-orbit servicing could lead to several advantages in terms of the cost-effectiveness, environmental sustainability, and strategic impact of future space missions. In fact, space-based servicing could play a fundamental role in the maintenance and upgrades of valuable orbiting assets, while also allowing the removal of space debris or potentially adversarial spacecraft.

Successfully designing and executing space servicing missions requires overcoming several major scientific and technological hurdles. The NASA Exploration and In-Space Services group at NASA's Goddard Space Flight Center has led the way in conceptualizing and implementing

technologies relevant to in-orbit servicing, assembly, and manufacturing. Reed (3) delineated the group's mission as follows:

- Advance the state of robotic servicing technology to enable routine servicing of satellites that were not originally designed with servicing in mind.
- Position the United States to be the global leader in in-space repair, maintenance, and satellite disposal.
- Help enable a future US industry for satellite servicing.

A recent report from the National Science and Technology Council (4) on the national strategy for in-space servicing, assembly, and manufacturing (ISAM) identified six strategic goals to realize the opportunities enabled by ISAM. The six goals are (a) advancing ISAM research and development, (b) prioritizing the expansion of scalable infrastructure, (c) accelerating the emerging ISAM commercial industry, (d) promoting international collaboration and cooperation to achieve ISAM goals, (e) prioritizing environmental sustainability, and (f) inspiring a diverse future workforce. In-space robotics technologies are indispensable for making this vision a reality.

Satellite servicing encompasses a wide range of uses that aim primarily to extend the satellite lifetime. Common services include visual inspection, scheduled maintenance, refueling, part replacement, repair of worn or broken components, and completion of failed deployment sequences, among others. Akin (5) proposed four broad servicing categories: dexterous servicing, simple servicing, inspection, and orbit reboost. The benefits of robotic servicing arise primarily from decreasing the risk to astronauts performing extravehicular activities or from increasing astronaut efficiency (6). Without the restriction of having human crew involved, robotic missions can also go beyond low Earth orbits to regions of higher radiation, or even operate in high-inclination polar orbits.

When planning a robotic servicing mission, a delicate balance is sought between system complexity and servicer capability. Bronez et al. (7) laid out a set of requirements that a servicer system would need to satisfy in order to accomplish on-orbit replacement of a malfunctioning component on a host satellite. As pointed out by Akin et al. (8), basic module-exchange servicers decrease the complexity of the servicing spacecraft, but this option is likely to require a more complex architecture of the serviced satellite (the host) in terms of electrical and mechanical connections. With increasing dexterity of the servicing satellite, the host satellite can remain closer to flight-proven heritage architectures and increase mission reliability. This increased dexterity can be provided through the on-orbit exchange of end-effector tools, such as those proposed by Akin (5) or, more recently, by Qu et al. (9). The price to pay for increased dexterity is a coupling between the dynamics of the robotic arm extending this tool and the satellite base that holds it. Considerations of conservation of angular momentum (made more pronounced by the use of smaller, more agile spacecraft with longer arms) make controlling a spacecraft with articulated arms a challenging proposition, especially when accounting for the limited onboard fuel. In addition, sophisticated sensing and control architectures need to be designed to enhance the flexibility of the servicer platform, account for diverse mission scenarios, and conform to numerous client configurations. The intricate dynamic coupling between the manipulator(s) and the satellite base, along with a variety of guidance, navigation, and control solutions, has been the subject of intense scrutiny from academia and industry alike (10). Understanding these components and their limitations is essential to the success of all SMRS missions that utilize one or more articulated arms.

1.2. A Brief Historical Review of In-Space Robotic Missions

Since the launch of the first space probes between the end of the 1950s and the early 1960s, a great part of the human endeavors in space has been made possible by orbiting machines

featuring some degree of autonomy. For this reason, unmanned space missions are usually referred to as robotic missions. Space robotics therefore gathers a broad family of autonomous systems, whose architectures are heavily dependent on the goals and requirements of each mission. Among these systems, exploration probes can be identified as traditional platforms, as opposed to planetary rovers and spacecraft-mounted manipulators, whose peculiar configurations and modus operandi more closely reflect the notion of a robot deployed in space. While this review is concerned primarily with the science and technology of satellite-mounted manipulators, rovers have been a key element in many planetary surface exploration missions, from the Soviet lunar Lunokhod program (11) up to the present NASA Mars robotic missions (12–15). Complex vehicle dynamics and control, motion planning and obstacle avoidance on rugged terrain, and tight mass and energy budgets are only some of the challenges one faces when designing a planetary rover. In this article, we do not delve further into rover robotic missions and focus instead specifically on space robotic manipulators; for a more detailed discussion of the role of rovers in prior planetary exploration missions, we direct readers to Reference 16.

The first free-flying robotic arm in orbit was Engineering Test Satellite No. 7 (ETS-VII), launched in 1997 by the National Space Development Agency of Japan. The goal of ETS-VII was to test robotic technology for unmanned on-orbit servicing. The mission envisaged two main subtasks: autonomous rendezvous/docking and robot experiments (17). Among the many tests, simultaneous base–manipulator control was performed, the robotic arm was successfully used for the capture of a floating target, and equipment change and fuel resupply experiments were conducted (18, 19). Moreover, fundamental theoretical results dealing with free-flying robot dynamics and control, such as the generalized Jacobian matrix (20) and the reaction null space (21), were validated in-flight, providing the space robotics community with a set of precious insights for the analysis of future missions.

The Shuttle Remote Manipulator System (SRMS, or Canadarm) was the first example of a robotic manipulator used in space to handle payloads and to perform satellite inspection, assembly, and servicing. After its first flight onboard the orbiter *Columbia* in 1981 during the Space Transportation System 2 (STS-2) mission, the SRMS became a key component in many of the subsequent missions during the 30-year Space Shuttle program. In particular, the Space Shuttle's robotic arm supported the astronauts during several Hubble Space Telescope servicing missions, enabled docking to the Russian space station during the Shuttle–Mir program, and played a key role in the on-orbit assembly of the ISS.

Inspired by the success of the original Canadarm, the Canadian Space Agency built the Space Station Remote Manipulator System (SSRMS, or Canadarm2), a 17-m-long robotic manipulator installed on the ISS that carries two identical end effectors, which are used to latch the manipulator itself to the station or to manipulate objects. The SSRMS has been used to berth vehicles to the ISS, move astronauts and supplies around, support scientific experiments, and maintain and upgrade the ISS. Both Canadarms were designed to be operated by the flight crews; in order to relieve the astronauts' workload, ground control of the Canadarm2 was also tested (22). The Canadarms provide a good example of the prospects related to the usage of manipulators in space; however, since their base-to-manipulator mass ratio is on the order of 200:1, the satellite-base displacement due to the manipulator motion is negligible, and the two systems can be thought of as mounted on a fixed base.

In addition to the Canadian SRMS and SSRMS, similar systems deployed onboard the ISS include the Japanese Experiment Module Remote Manipulator System (23) and the European Robotic Arm (24). These systems were installed on the Japanese Experiment Module and the Russian Orbital Segment in 2008 and 2021, respectively.

In addition to these efforts, back in 1993, after a seven-year development phase, the German Aerospace Center's Robot Technology Experiment (ROTEX) (25) was flown onboard the Space Shuttle *Columbia* during the STS-55 mission. ROTEX was a small multisensory robot mounted inside the D-2 Spacelab whose mission consisted of three experimental tasks: the assembly of a truss structure, the connection and disconnection of an orbital replacement unit, and—for the first time in the history of spaceflight—the capture of a floating object. Such experiments were carried out using a variety of control modes, including onboard teleoperation [astronauts using a hand controller with six degrees of freedom (DOFs)], teleoperation from the ground, and sensorbased offline programming. In the last, the robot maneuver was first performed on the ground in a graphics simulator, and the simulated sensor data then served as a reference during the execution phase. During the in-flight experiment, the robot controller compared the information obtained from the graphics simulation with the real-time sensor data.

A follow-up German Aerospace Center experiment consisted of a two-DOF torque-controlled robot, ROKVISS (26), that was installed on the Russian Service Module of the ISS in 2005. Multiple operational modes were tested to cope with different communication delays. A telepresence mode through force-feedback control to the remote operator was demonstrated for delays less than 500 ms, while longer delays were compensated through a time-domain passivity controller that ensured the stability of the operator-robot loop. Experiments were also performed within the so-called telerobotic and automatic modes, where the first mode still required direct radio contact between the ground station and the ISS, while the automatic mode handled predefined trajectories in the absence of a communication window.

In 2007, DARPA executed Orbital Express, an on-orbit servicing mission, consisting of a servicing platform (ASTRO) and a next-generation prototype serviceable satellite (NEXTSat). The mission aimed to investigate the feasibility of establishing an autonomous, cost-effective on-orbit servicing infrastructure (27). Several key technologies were demonstrated throughout the mission, including standard satellite servicing interfaces, autonomous rendezvous and proximity operations, and transfer of fluid and orbital replacement units.

More recently, another DARPA program, Front-End Robotics Enabling Near-Term Demonstration (FREND), focused on the demonstration of autonomous rendezvous and docking aimed at the capture and orbit elevation of geosynchronous equatorial orbit (GEO) communications satellites and their possible repositioning to gain coverage of specific regions (28). A follow-up to FREND is the Robotic Servicing of Geosynchronous Satellites (RSGS) program, whose goal is "to create a dexterous robotic operational capability in Geosynchronous Orbit, that can both provide increased resilience for the current US space infrastructure, and be the first concrete step toward a transformed space architecture with revolutionary capabilities" (29, slide 12), a statement that closely aligns with the National Space Policy published in 2010 (30).

Similarly to FREND and RSGS, the DARPA Phoenix project (31) sought to demonstrate cost-effective on-orbit assembly and payload delivery for GEO satellites. Three key elements of Phoenix were the presence of a main tender satellite with a dexterous manipulator and sufficient fuel to service multiple GEO satellites, cellularized elements (satlets) as modular low-cost satellite architectural units, and a standardized Payload Orbital Delivery module designed to carry different kinds of payloads into orbit aboard communication satellites. The technologies investigated during the FREND and Phoenix programs were tested in the laboratory but were never sent into orbit.

In 2016, the China Academy of Launch Vehicle Technology and the Harbin Institute of Technology launched the Aolong-1 satellite onboard the Chinese Long March 7 rocket (32). Aolong-1 consisted of a small satellite equipped with a robotic arm. According to the available

information, the goal of the mission was to perform active debris removal by grabbing space debris and accelerating it toward the atmosphere.

The previous on-orbit robotic activities considered mainly the interactions with human-made objects. One of the primary benefits of robot-wielding satellites will be the capability to capture an Earth-threatening asteroid, possibly redirecting it toward a safe zone. In fact, Brophy et al. (33) and Strange et al. (34) described NASA's Asteroid Redirect Robotic Mission as a variant of this technology in which an asteroid is instead captured and carried into cislunar space.

2. SPACECRAFT-MOUNTED ROBOTIC MODELING

The modeling of the dynamics of spacecraft-mounted robotic manipulators is of the utmost importance for the successful use of robots in space. The principles of conservation of linear and angular momentum invalidate the simple, kinematically driven approaches that are typically used for fixed-base robotic manipulators. In this section, we discuss the main results dealing with the modeling and control of SMRSs. In the next section, we introduce a novel description, based on dual quaternion algebra, that is more suitable for coordinated maneuvering of spacecraft-mounted robotic manipulators by treating the translational and rotational motion in a combined, coordinated manner.

We classify SMRSs as free-flying or free-floating according to the following criteria. The free-flying case reflects the scenario when the satellite base is actively controlled by thrusters in translation, orientation, or both. In this case, the center of mass of the spacecraft–manipulator system can translate as a result of the action exerted by the thrusters. In a free-floating spacecraft scenario, by contrast, all external thrusters at the base are turned off, and as a result, both the linear and angular momenta of the whole SMRS are preserved. In a free-floating mode, the center of mass of the system cannot translate, although the spacecraft translates and rotates as a result of its reactions to manipulator motions. Obviously, the free-flying case offers the greatest flexibility of on-orbit servicing tasks, but it has the drawback of propellant usage.

2.1. The Free-Flying Case

Bronez et al. (7) gave an example of a fully controlled free-flying SMRS in which they addressed the specification requirements for a robotic servicer in charge of transferring a payload between a space station and a nearby satellite in need of servicing. Among the various requirements (propulsion, guidance, navigation, etc.), they focused their attention on a system consisting of multiple dexterous manipulators, whose goal is to provide assistance during high-precision docking maneuvers, payload transfer, inspection, interaction with the space station's main manipulator system, and so on. Reuter et al. (35) described an analogous concept in which the system is designed to retrieve objects or astronauts after accidental untethering from the space station.

Two main modeling approaches are available for the analysis and simulation of the dynamics of a free-flying multibody system: a Lagrangian approach and a recursive Newton–Euler approach. The former entails a laborious closed-form derivation of the system's mass matrix, nonlinear velocity terms, and generalized forces, resulting in a rigorous formulation that is suitable mostly for analysis purposes, whereas the latter relies on the recursive application of the Newton–Euler dynamic equations and has been widely adopted to build numerical simulations of free-flyers characterized by complex configurations with multiple manipulators, different types of joints, and so on.

Several foundational studies in space robotics hinge on the closed-form (Lagrangian) approach. Moosavian & Papadopoulos (36) described the system's kinematics through the direct path method (37) and subsequently exploited the position and velocity analyses to compute the overall kinetic energy, to which they applied the Lagrange formalism. Papadopoulos (38) presented an

alternative closed-form analysis where kinematic modeling is based on barycentric vectors, a set of body-fixed quantities encompassing information on both the geometry and the mass distribution of the system. Although more demanding from a computational viewpoint, the use of barycentric quantities eventually leads to advantages in terms of control design (37). Dubowsky et al. (39) obtained the nine nonlinear dynamic equations describing a three-DOF manipulator mounted on a six-DOF spacecraft via a Lagrangian formulation that includes a $9 \times 9 \times 9$ tensor expressing the Coriolis-like terms. These equations are, however, significantly simplified when used to describe a stabilized spacecraft for which the time derivatives of the generalized coordinates of the base can be set to zero.

The free-flyers' dynamics may also be expressed through the recursive application of the Newton–Euler equations to each of the bodies composing the SMRS. Such a formulation is well suited to the representation of complex orbiting manipulators with multiple appendages that may be subject to different sets of forces or torques (actuations, environmental disturbances, contact wrenches, etc.). Egeland & Sagli (40) adopted the recursive framework and used it to develop a control scheme for coordinating the motion of the satellite and the robot end effector. The proposed controller was then simulated using a 12-DOF model, whose inverse dynamics was calculated recursively according to Reference 41. Equivalent recursive formulations based on the so-called Newton–Euler algorithm have been widely adopted by the space robotics community due to their ease of implementation, flexibility, and computational efficiency. For example, Carignan & Akin (42) gave a thorough overview in which they leveraged the typical Newton–Euler outward–inward recursions in order to model the dynamic coupling between a free-flying base and a system of four manipulators.

In the context of recursive formulations, compactness and computational efficiency have also been pursued in different works. In particular, Featherstone (43, chapter 9) resorted to spatial operator algebra and specialized the recursive Newton–Euler algorithm to spacecraft-mounted manipulators.

Independently of the method used, the aforementioned approaches result in a dynamic equation of the following form (see, e.g., 36, 44):

$$\begin{bmatrix} M_{\mathrm{B}_{1}} & M_{\mathrm{B}_{1},\mathrm{m}} \\ M_{\mathrm{B}_{1},\mathrm{m}}^{\mathsf{T}} & M_{\mathrm{m}} \end{bmatrix} \begin{bmatrix} \dot{\boldsymbol{\omega}}_{\mathrm{B}_{1}/\mathrm{I}} \\ \ddot{\Gamma} \end{bmatrix} + \begin{bmatrix} c_{\mathrm{b}} \\ c_{\Gamma} \end{bmatrix} = \begin{bmatrix} \boldsymbol{W}_{\mathrm{B}_{1}} \\ \tau \end{bmatrix} + \begin{bmatrix} R_{\mathrm{B}_{N}/\mathrm{B}_{1}}^{\mathsf{T}} \\ J_{\mathrm{m}}^{\mathsf{T}} \end{bmatrix} \boldsymbol{W}_{\mathrm{B}_{N},\mathrm{ext}},$$
 1.

where $M_{\rm B_1}$ is the base inertia matrix; $M_{\rm B_1,m}$ expresses the inertial coupling between the base and the manipulator; $M_{\rm m}$ is the fixed-base inertia matrix of the manipulator; $\omega_{\rm B_1/I}$ and $\dot{\Gamma}$ are the velocity of the base and the joint rates, respectively; $c_{\rm b}$ and $c_{\rm \Gamma}$ are the vectors of the Coriolis and centrifugal forces acting on the base and on the manipulator, respectively; $W_{\rm B_1}$ is the wrench (force and torque) acting on the base (due to thrusters and/or reaction/momentum wheels); τ collects the torques applied by the joint motors; $R_{\rm B_N/B_1}$ encodes the wrench transformation between the end effector and the base frame; $J_{\rm m}$ is the manipulator Jacobian; and $W_{\rm B_N,ext}$ is the wrench generated by the end effector coming into contact with an external object.

Within the free-flying class, the satellite actuators can be exploited according to a whole gamut of maneuvering strategies, from simple station-keeping tasks to more complex base/manipulator coordinated motions. Seddaoui & Saaj (45) proposed a specific classification where a fully coordinated motion is referred to as controlled floating. They maintained a distinction between a controlled-floating space robot and a more static free-flying type of operation, where the latter is seen as restricted to station-keeping duties or to limited changes in the pose of the satellite. To achieve precise pose control during a servicing operation within the controlled-floating scenario, Seddaoui et al. (46) developed a refined dynamic model by deriving the equations of motion for a

controlled-floating space robot in the target rotating orbit frame, hence taking into account additional dynamic coupling effects due to orbital mechanics. As a consequence of this modeling approach, the center of mass of the overall system is not fixed anymore, even in the absence of actuation. Because of this, many of the traditional results that exploit momentum conservation are no longer valid in the controlled-floating space robot framework.

2.2. The Free-Floating Case

The free-floating case is much more challenging, owing to momentum conservation considerations. The most significant result concerning free-floating systems is perhaps the one presented by Umetani & Yoshida (20, 47). The authors derived an extended Jacobian matrix to obtain the Cartesian rate of the end effector as a result of the angular velocity of the base and the angular rates of the manipulator joints:

$$\boldsymbol{\omega}_{\mathrm{B_N/I}} = \begin{bmatrix} v_{\mathrm{B_N/I}} \\ \omega_{\mathrm{B_N/I}} \end{bmatrix} = \bar{\mathrm{J}}(\Gamma)\dot{\Gamma} + \boldsymbol{\omega}_{\mathrm{G/I}}, \qquad 2.$$

where $v_{B_N/I}$ and $\omega_{B_N/I}$ are the linear and angular task-space velocities of the end effector, respectively; $\Gamma = (\Gamma_s, \Gamma_m)$, with $\Gamma_s = (\alpha, \beta, \gamma)$, represents the attitude angles of the main body; $\Gamma_m = (\Gamma_1, \ldots, \Gamma_N)$ represents the robot joint angles; $\omega_{G/I}$ is an initial motion of the system center of mass; and \bar{J} is the extended Jacobian matrix. Equation 2 can be rewritten as

$$\boldsymbol{\omega}_{\mathrm{By/I}} = \bar{J}_{\mathrm{s}} \dot{\Gamma}_{\mathrm{s}} + \bar{J}_{\mathrm{m}} \dot{\Gamma}_{\mathrm{m}} + \boldsymbol{\omega}_{\mathrm{G/I}},$$
 3.

where \bar{J}_s and \bar{J}_m highlight the contributions of the satellite and the manipulator, respectively. The extended Jacobian cannot be directly inverted, since the number of unknowns (the angular rates of the base and the rates of the robot joints) is, in general, greater than the number of available equations. Therefore, the authors made use of the momentum conservation equation, stated as $M_{\rm B_1}\dot{\Gamma}_s + M_{\rm m}\dot{\Gamma}_m = L_0$, where $M_{\rm B_1}$ and $M_{\rm m}$ are the satellite and manipulator parts of the system's inertia matrix, respectively, and L_0 is the initial momentum. The unknown satellite angular rate $\dot{\Gamma}_s$ can be retrieved from the momentum equation as follows:

$$\dot{\Gamma}_{\rm s} = -M_{\rm B_1}^{-1} M_{\rm m} \dot{\Gamma}_{\rm m} + M_{\rm B_1}^{-1} L_0. \tag{4}$$

Substituting Equation 4 into Equation 3 enables the rate of the end effector to be uniquely expressed as a function of the manipulator joint rates:

$$\omega_{\rm B_N/I} = \bar{\rm J}^* \dot{\Gamma}_{\rm m} + \omega_{\rm G/I} + \bar{\rm J}_{\rm s} M_{\rm B_1}^{-1} L_0,$$
 5.

where $\bar{J}^* = \bar{J}_m - \bar{J}_s M_{B_1}^{-1} M_m$ is the generalized Jacobian matrix. In Equation 5, the purely kinematic relationship originally expressed in Equation 2 has been enriched with dynamic information that takes into account the base–manipulator interaction.

Papadopoulos & Dubowsky (48) described a set of singular points for the generalized Jacobian matrix. These points cannot be determined uniquely from the kinematic configuration of the manipulator, as they also depend on the history of the spacecraft attitude, which, in turn, is determined by the path taken by the robot end effector. Such singular configurations are referred to as dynamic singularities. Papadopoulos & Dubowsky (48) proved that the inertial workspace of a free-floating space manipulator can be divided into two regions: the path-dependent workspace and the path-independent workspace. The first is the union of the reachable workspace locations that may lead to dynamic singularities, depending on the path of the end effector, while the second is the subset of the inertial workspace where dynamic singularities do not arise, independently from the path taken.

The concept of a virtual manipulator was introduced by Vafa & Dubowsky (49–51). The virtual manipulator is connected through a spherical joint to the virtual ground (the center of mass of the SMRS), whose rotations represent the inertial rotations of the base. Rotations and displacements about virtual revolute or prismatic joints represent equivalent actual motions about the spacecraft joints. The lengths of the links of the virtual manipulator are related through a function of the mass of each of the links of the actual spacecraft and the SMRS geometry. Vafa & Dubowsky (52) claimed that the virtual manipulator can be used to simplify the inverse kinematics problem and the computation of the system workspace, as well as to simplify the analysis, design, control, and planning of robotic manipulators in space. For instance, in the case in which the attitude of the base is fixed, the workspace for the virtual manipulator, computed through conventional fixedbase methods, is equivalent to the workspace of the actual manipulator. Furthermore, since the virtual ground is fixed in inertial space, the inverse dynamics problem becomes a simple inverse kinematics problem, as with a fixed-base manipulator. Finally, for a desired change in the attitude of the base represented in terms of Euler angles, a method that relies on the cyclic motion of the generalized joint coordinate was suggested. This allows for general joint trajectories to be realized, albeit with frequent pauses to reorient the spacecraft base as needed.

An earlier study by Longman (53) investigated the dynamics, kinematics, inverse kinematics, and robot workspace for the case of a free-floating spacecraft. The author also postulated that any attitude for the base can be achieved by actuating the robotic arm. The same work showed that the reachable workspace of the robot arm is a sphere and that, for the majority of cases, this region is larger than that for the case in which the attitude of the base is constant or inertially fixed.

In a different vein, Dubowsky & Torres (54) made use of the disturbance map, originally proposed by Vafa & Dubowsky (49), and the enhanced disturbance map for path-planning purposes. These maps can be computed from knowledge of the configuration-dependent mass matrix of the whole system relative to the spacecraft body axes.

In the rest of this article, we revisit the modeling of an SMRS for the free-flying case and present an alternative method to derive the governing kinematic and dynamic equations under minimal assumptions, using hypercomplex number theory, specifically quaternions and dual quaternions. While the former have been used extensively for many years to describe the kinematics of rotating spacecraft owing to their nice property of singularity-free representation of rotations, the use of the latter in the spacecraft robotics community is more recent, although the usefulness of dual quaternions in ground-based robotic applications has been known for some time (55, 56).

The main benefit from the use of dual quaternions in SMRS modeling is that they can describe the combined rotational and translational motion in a single (scalar) quantity, without resorting to artificial assumptions about decoupling the two. The fact that dual quaternions in spacecraft applications have not been as widely adopted as regular quaternions can be traced to the traditional mode of satellite operations, which, until recently, assumed primarily that the satellite remains in its own orbit; therefore, only attitude control and reorientation were of interest. As proximity operations are receiving renewed interest, there is a need for spacecraft to perform more complex maneuvers that include both rotation and translation at the same time. Dual quaternions offer a nice and compact mathematical description of this combined motion.

3. MATHEMATICAL PRELIMINARIES

Before embarking on the derivation of the equations of an SMRS in terms of dual quaternions, for the purpose of completeness, in the next two sections we provide a brief overview of quaternions, dual quaternions, and their associated algebras.

Table 1 Quaternion operations

Operation	Definition
Addition	$a + b = (a_0 + b_0, \bar{a} + \bar{b})$
Multiplication by a scalar	$\lambda a = (\lambda a_0, \lambda a)$
Multiplication	$ab = (a_0b_0 - \bar{a} \cdot \bar{b}, a_0\bar{b} + b_0\bar{a} + \bar{a} \times \bar{b})$
Conjugate	$a^* = (a_0, -\bar{a})$
Dot product	$a \cdot b = (a_0 b_0 + \bar{a} \cdot \bar{b}, 0_{3 \times 1}) = \frac{1}{2} (a^* b + b^* a)$
Cross product	$a \times b = (0, a_0 \bar{b} + b_0 \bar{a} + \bar{a} \times \bar{b}) = \frac{1}{2} (ab - b^* a^*)$
Norm	$ a = \sqrt{a \cdot a}$
Matrix-quaternion multiplication ^a	$M*a = (M_{11}a_0 + M_{12}\bar{a}, M_{21}a_0 + M_{22}\bar{a})$

^aAssume a matrix $M \in \mathbb{R}^{4\times 4}$ with $M_{11} \in \mathbb{R}, M_{12} \in \mathbb{R}^{1\times 3}, M_{21} \in \mathbb{R}^{3\times 1}$, and $M_{22} \in \mathbb{R}^{3\times 3}$.

3.1. Quaternions

Quaternions extend the well-known imaginary unit $j = \sqrt{-1}$, forming an algebra over the field of real numbers defined as $\mathbb{H} \triangleq \{q = q_0 + q_1i + q_2j + q_3k : i^2 = j^2 = k^2 = ijk = -1, \ q_0, q_1, q_2, q_3 \in \mathbb{R} \}$. In practice, quaternions are often referred to by their scalar and vector parts as $q = (q_0, \overline{q})$, where $q_0 \in \mathbb{R}$ and $\overline{q} = (q_1, q_2, q_3) \in \mathbb{R}^3$ are the scalar and vector parts of q, respectively. The quaternion expresses a general three-dimensional rotation as a rotation at an angle ϕ about a specific eigenaxis $\hat{\eta}$ as follows:

$$q = (q_0, \bar{q}) = \left(\cos\frac{\phi}{2}, \hat{\eta}\sin\frac{\phi}{2}\right).$$
 6.

Some common properties of quaternion algebra are summarized in **Table 1**. Unit quaternions—that is, quaternions that satisfy the constraint $q \cdot q = ||q||^2 = 1$ —can be used to describe the orientation between two frames. In particular, the attitude (or orientation) of frame X with respect to frame Y can be expressed by the unit quaternion $q_{X/Y}$ that satisfies the identity $q_{X/Y}^*q_{X/Y} = q_{X/Y}q_{X/Y}^* = 1$, where $1 = (1, \bar{0}_{3\times 1})$. Given quaternions $q_{Y/X}$ and $q_{Z/Y}$, the quaternion describing the rotation from X to Z is given by $q_{Z/X} = q_{Y/X}q_{Z/Y}$.

Three-dimensional vectors can be also interpreted as special cases of quaternions. Specifically, given $\bar{s}^X \in \mathbb{R}^3$, a vector expressed in frame X has quaternion representation $s^X = (0, \bar{s}^X) \in \mathbb{H}^v$, where \mathbb{H}^v is the set of vector quaternions, defined as $\mathbb{H}^v \triangleq \{(q_0, \overline{q}) \in \mathbb{H} : q_0 = 0\}$ (for further discussion, see 57).

3.2. Dual Quaternions

Dual quaternions extend quaternions using dual number theory (58, 59). Specifically, letting the dual unit be defined as the scalar such that $\epsilon^2 = 0$ with $\epsilon \neq 0$, the dual quaternion algebra over the field of real numbers is defined as $\mathbb{H}_d = \{q = q_r + \epsilon q_d : q_r, q_d \in \mathbb{H}\}$, where ϵ is the dual unit and q_r and q_d are the real part and the dual part, respectively, of the dual quaternion q. The main properties of the dual quaternion algebra are listed in **Table 2**. Analogous to the set of vector quaternions \mathbb{H}^v , we can define the set of vector dual quaternions as $\mathbb{H}^v_d \triangleq \{q = q_r + \epsilon q_d : q_r, q_d \in \mathbb{H}^v\}$. These are the set of two (regular) vectors combined together using the dual unit.

Whereas unit quaternions can efficiently represent rotations, unit dual quaternions (i.e., dual quaternions whose real part is a unit quaternion) can efficiently represent rotations and translations. Specifically, given two frames—say, I and B—the dual quaternion describing the relative pose of frame B relative to frame I is given by

$$\mathbf{q}_{\rm B/I} = q_{\rm B/I,r} + \epsilon q_{\rm B/I,d} = q_{\rm B/I} + \epsilon \frac{1}{2} r_{\rm B/I}^{\rm I} q_{\rm B/I} = q_{\rm B/I} + \epsilon \frac{1}{2} q_{\rm B/I} r_{\rm B/I}^{\rm B},$$
 7.

Table 2 Dual quaternion operations

Operation	Definition
Addition	$a + b = (a_{r} + b_{r}) + \epsilon (a_{d} + b_{d})$
Multiplication by a scalar	$\lambda \mathbf{a} = (\lambda a_{\rm r}) + \epsilon (\lambda a_{\rm d})$
Multiplication	$ab = (a_{\rm r}b_{\rm r}) + \epsilon(a_{\rm d}b_{\rm r} + a_{\rm r}b_{\rm d})$
Conjugate	$a^* = (a_{\rm r}^*) + \epsilon(a_{\rm d}^*)$
Dot product	$\boldsymbol{a} \cdot \boldsymbol{b} = (a_{\mathrm{r}} \cdot b_{\mathrm{r}}) + \epsilon (a_{\mathrm{d}} \cdot b_{\mathrm{r}} + a_{\mathrm{r}} \cdot b_{\mathrm{d}}) = \frac{1}{2} (\boldsymbol{a}^* \boldsymbol{b} + \boldsymbol{b}^* \boldsymbol{a})$
Cross product	$\mathbf{a} \times \mathbf{b} = (a_{\mathrm{r}} \times b_{\mathrm{r}}) + \epsilon (a_{\mathrm{d}} \times b_{\mathrm{r}} + a_{\mathrm{r}} \times b_{\mathrm{d}}) = \frac{1}{2} (\mathbf{ab} - \mathbf{b}^* \mathbf{a}^*)$
Circle product	$\boldsymbol{a} \circ \boldsymbol{b} = (a_{\mathrm{r}} \cdot b_{\mathrm{r}} + a_{\mathrm{d}} \cdot b_{\mathrm{d}}) + \epsilon 0$
Swap	$(a)^{S} = a_{d} + \epsilon a_{r}$
Norm	$ a = \sqrt{a \circ a}$
Vector part	$\operatorname{vec}(\boldsymbol{a}) = (0, \overline{a_{r}}) + \epsilon(0, \overline{a_{d}})$

where $r_{Y/Z}^X = (0, \bar{r}_{Y/Z}^X)$ and $\bar{r}_{Y/Z}^X \in \mathbb{R}^3$ is the translation vector from the origin of the Z frame to the origin of the Y frame expressed in the X frame. Note that the dual part of $q_{B/I}$ (i.e., $q_{B/I,d} = \frac{1}{2} r_{B/I}^I q_{B/I} = \frac{1}{2} q_{B/I} r_{B/I}^B$) is a representation of the position of the body frame with respect to the inertial frame that is expressed in neither the B frame nor the B frame.

Given the unit dual quaternion $q_{\rm B/I} = q_{\rm B/I,r} + \epsilon q_{\rm B/I,d}$, $r_{\rm B/I}^{\rm B}$ and $r_{\rm B/I}^{\rm I}$ can be recovered through the expressions

$$r_{\rm B/I}^{\rm I} = 2q_{\rm B/I,d}q_{\rm B/I,r}^*, \qquad r_{\rm B/I}^{\rm B} = 2q_{\rm B/I,r}^*q_{\rm B/I,d}.$$
 8.

It can be easily observed that

$$q_{B/I,r} \cdot q_{B/I,r} = 1, \qquad q_{B/I,r} \cdot q_{B/I,d} = 0,$$
 9.

and hence $q \cdot q = q^*q = 1$. Since only six elements are necessary to represent a pose, a unit dual quaternion, which has eight elements, must satisfy two algebraic constraints. These are exactly the constraints given in Equation 9. From these constraints, and assuming that $-180^{\circ} < \phi < 180^{\circ}$, the scalar parts of the real and dual parts of a unit dual quaternion can be computed from their respective vector parts via

$$q_{r,0} = \sqrt{1 - \|\overline{q}_r\|^2}, \qquad q_{d,0} = -\frac{\overline{q}_r^{\mathsf{T}} \overline{q}_d}{q_{r,0}}.$$
 10.

Analogous to normalization in the space of quaternions, a dual quaternion can be forced to satisfy the unit and orthogonality constraints in Equation 9. For a given unit dual quaternion $q \in \mathbb{H}_d$, one way to enforce the constraints in Equation 9 is to set

$$q_{\rm r} = \frac{q_{\rm r}}{\|q_{\rm r}\|}, \qquad q_{\rm d} = q_{\rm d} - \frac{q_{\rm r}}{\|q_{\rm r}\|^2} (q_{\rm r} \cdot q_{\rm d}).$$
 11.

4. INTEGRATED MODELING OF SPACECRAFT-MOUNTED ROBOTIC SYSTEMS

We will model an N-body SMRS as a graph $\mathcal{G} = \mathcal{G}(\mathcal{V}, \mathcal{E})$, where \mathcal{V} is the set of vertices and \mathcal{E} represents the set of edges. The nodes of the graph \mathcal{G} represent the rigid bodies of the SMRS, consisting of the spacecraft base and the links of the manipulator(s), while the edges represent the joints connecting the various rigid bodies. In general, \mathcal{G} is an acyclic graph (i.e., a tree), with the various tree branches emanating from a single root node representing the spacecraft base. For SMRS configurations involving multiple manipulators, however, cycles may exist; assuming \mathcal{G} is

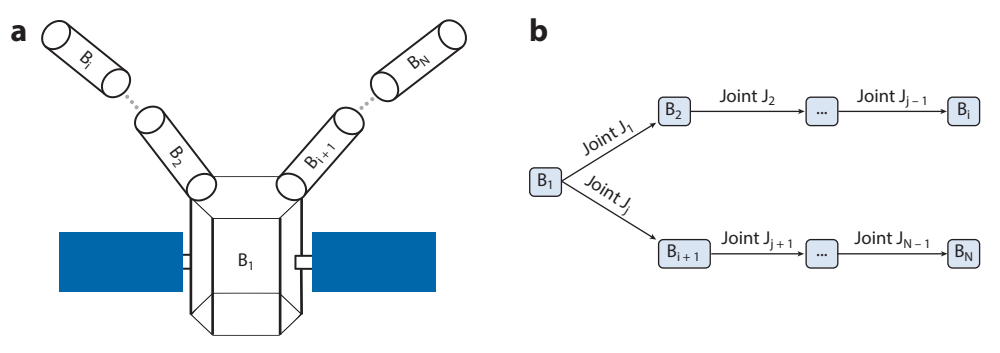


Figure 1

(a) A conceptual architecture for a satellite with a two-arm spacecraft-mounted robotic system. (b) The same architecture as a rooted tree with labeled vertices (nodes) and edges. Figure adapted from Reference 61 (CC BY 4.0).

a general graph (including cycles) provides the flexibility needed to handle coordinated manipulation tasks involving multiple arms. **Figure 1***a* shows an example of the labeling for the case of a satellite with a two-arm SMRS; **Figure 1***b* shows the same configuration with labeled vertices (nodes) and edges.

Corresponding to the graph \mathcal{G} is the incidence matrix C that contains the information about the connectivity between the joints and the bodies of the SMRS. Specifically, the rows of the incidence matrix represent rigid bodies, while the columns represent joints. Thus, the entry C_{ij} of C indicates the relationship between rigid body i and joint j as follows:

$$C_{ij} \triangleq \begin{cases} 1, & \text{if body i is distal and joint j is proximal,} \\ 0, & \text{if body i is not connected to joint j,} \\ -1, & \text{if body i is proximal and joint j is distal,} \end{cases}$$

where the relative positions (proximal/distal) are with respect to the satellite base.

In addition to the inertial frame I and the satellite-base frame B_1 , we introduce body-fixed frames B_i for each body having as its origin the center of mass O_{B_i} of body B_i and joint frames J_j with origin O_{J_j} of joint J_j (see **Figure 2**). Using this notation, we can write, for instance, the dual velocity of joint J_j with respect to body B_i , expressed in the joint J_j -frame coordinates, as ω_{J_j/B_i} ,

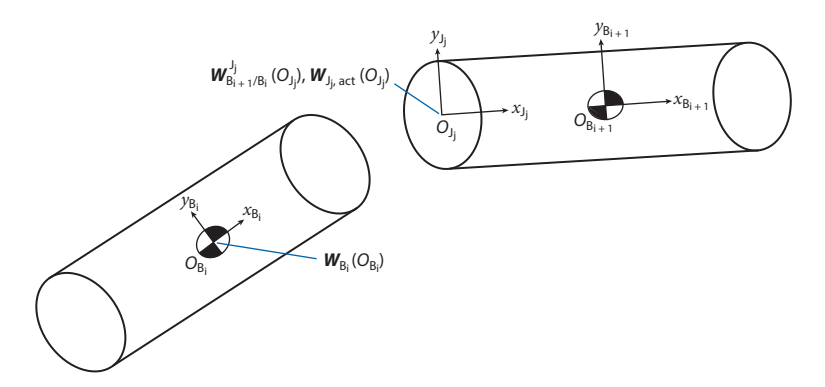


Figure 2

Body frame labeling and wrench definition at joint J_j between bodies B_i and B_{i+1} . Figure adapted from Reference 61 (CC BY 4.0).

NOTATION

The dual velocity of the Y frame with respect to the Z frame, expressed in X-frame coordinates, is defined as

$$\boldsymbol{\omega}_{\text{Y/Z}}^{\text{X}} = \boldsymbol{q}_{\text{X/Y}}^* \boldsymbol{\omega}_{\text{Y/Z}}^{\text{Y}} \boldsymbol{q}_{\text{X/Y}} = \boldsymbol{\omega}_{\text{Y/Z}}^{\text{X}} + \epsilon \big(v_{\text{Y/Z}}^{\text{X}} + \boldsymbol{\omega}_{\text{Y/Z}}^{\text{X}} \times r_{\text{X/Y}}^{\text{X}} \big),$$

where $\omega_{Y/Z}^X$ is equal to $(0, \bar{\omega}_{Y/Z}^X)$; $v_{Y/Z}^X$ is equal to $(0, \bar{v}_{Y/Z}^X)$; $\bar{\omega}_{Y/Z}^X$ and $\bar{v}_{Y/Z}^X \in \mathbb{R}^3$ are, respectively, the angular and linear velocities of the Y frame with respect to the Z frame expressed in X-frame coordinates; and $r_{X/Y}^X$ is equal to $(0, \bar{r}_{X/Y}^X)$, where $\bar{r}_{X/Y}^X \in \mathbb{R}^3$ is the position vector from the origin of the Y frame to the origin of the X frame expressed in X-frame coordinates. If the frames X and Y coincide, we drop the superscript—that is, we write $r_{Y/Z}$ instead of $r_{Y/Z}^Y$, and so on. In particular, the dual velocity of a rigid body assigned to frame B_i , located at the center of mass of body i, with respect to the inertial frame I, expressed in the B_i -frame coordinates, is denoted as

$$\boldsymbol{\omega}_{\mathrm{B_i/I}} = \omega_{\mathrm{B_i/I}} + \epsilon \, v_{\mathrm{B_i/I}}.$$

whereas the dual velocity of body B_i with respect to the inertial frame, expressed in the body B_i -frame coordinates, is given as $\omega_{B_i/I}$ (see also the sidebar titled Notation).

In the rest of the article, in order to keep the notation as concise as possible, we deal only with the special case of a single manipulator. The general case can be easily derived from the single-manipulator case; interested readers can find the details for the general, multimanipulator SMRS configuration in Reference 60.

4.1. Kinematics

The kinematics of an SMRS are fully characterized by the kinematics of the satellite base and the kinematics of the joints. The pose of the satellite base with respect to the inertial frame is given by (see also Equation 7) the dual quaternion

$$q_{\rm B_1/I} = q_{\rm B_1/I} + \epsilon \frac{1}{2} q_{\rm B_1/I} r_{\rm B_1/I},$$
 13.

where $r_{\rm B_1/I} = (0, \bar{r}_{\rm B_1/I})$, which evolves according to

$$\dot{q}_{\rm B_1/I} = \frac{1}{2} q_{\rm B_1/I} \omega_{\rm B_1/I},$$
 14.

where $\omega_{B_1/I}$ is the dual velocity of the base, given by

$$\boldsymbol{\omega}_{\mathrm{B}_{1}/\mathrm{I}} = \omega_{\mathrm{B}_{1}/\mathrm{I}} + \epsilon \, v_{\mathrm{B}_{1}/\mathrm{I}}. \tag{15}$$

The joint dual velocity expressed in joint coordinates can be determined easily from the dual velocities of the adjacent bodies as follows:

$$\omega_{J_{j}/B_{i}} = q_{B_{i+1}/J_{j}}\omega_{B_{i+1}/I}q_{B_{i+1}/J_{i}}^{*} - q_{J_{i}/B_{i}}^{*}\omega_{B_{i}/I}q_{J_{j}/B_{i}}.$$
16.

Although the joint dual velocities suffice to describe the relative motion between the two connecting bodies, it is often much more intuitive and easier to work with the generalized coordinates that parameterize the free DOFs of each joint. In this case, the joint dual velocities are related to the derivatives of the generalized coordinates of each joint by a simple projection (see the sidebar titled Joints along with **Table 3**).

Assuming an SMRS consisting of N bodies, let $\Gamma \triangleq (\Gamma_1, \dots, \Gamma_j, \dots, \Gamma_{N-1}) \in \mathbb{R}^D$ be the collection of all generalized coordinates, where $D = \sum_{j=1}^{N-1} d_j$, with d_j being the DOF of joint J_j .

JOINTS

Joints connect the various links of an SMRS and constrain their relative motion. Different joints constrain the motion along different directions (i.e., DOFs). Generalized coordinates are used to describe the kinematic motion along the remaining DOFs. **Table 3** summarizes the primary joint types and their corresponding generalized coordinate parameters.

Table 3 The primary joint types and their generalized coordinate parameters

Joint type	Generalized coordinate parameterization	d _j (DOFs)
Revolute	$\theta_{J_i/B_i} \in \mathbb{R}^1$	1
Prismatic	$z_{\mathrm{J_{j}/B_{i}}} \in \mathbb{R}^{1}$	1
Spherical	$\left[\phi_{\mathrm{J_{j}/B_{i}}}, \theta_{\mathrm{J_{j}/B_{i}}}, \psi_{\mathrm{J_{j}/B_{i}}}\right]^{T} \in \mathbb{R}^{3}$	3
Cylindrical	$\left[\theta_{J_j/B_i}, z_{J_j/B_i}\right]^{T} \in \mathbb{R}^2$	2
Cartesian	$\left[x_{J_i/B_i}, y_{J_i/B_i}, z_{J_i/B_i}\right]^T \in \mathbb{R}^3$	3

Abbreviation: DOF, degree of freedom.

Specifically, we can write the relationship between the generalized speeds and the corresponding dual velocities for each joint as

$$\dot{\Gamma}_{\mathbf{j}} = \Pi_{\mathbf{j}} \circledast \boldsymbol{\omega}_{\mathbf{J}_{\mathbf{i}}/\mathbf{B}_{\mathbf{i}}}, \qquad 17.$$

where $\circledast : \mathbb{R}^{d_j \times 8} \times \mathbb{H}^v_d \to \mathbb{R}^{d_j}$ maps ω_{J_j/B_i} via the projection matrix $\Pi_j \in \mathbb{R}^{d_j \times 8}$ depending on the type of joint J_i , the exact expression of which is given in Reference 61.

The state vector of the system, henceforth denoted by \mathbf{x} , is given by the pose (orientation and location) of the satellite base represented by $\mathbf{q}_{B_1/I}$; its linear and angular velocities, captured by $\boldsymbol{\omega}_{B_1/I}$; and the generalized coordinates Γ and speeds $\dot{\Gamma}$ of all the joints. That is,

$$\mathbf{x} \triangleq (\mathbf{q}_{\mathrm{B}_{1}/\mathrm{I}}, \Gamma, \boldsymbol{\omega}_{\mathrm{B}_{1}/\mathrm{I}}, \dot{\Gamma}).$$
 18.

The collection of all body dual velocities is represented by v, as follows:

$$\boldsymbol{v} = (\boldsymbol{\omega}_{B_1/I}, \dots, \boldsymbol{\omega}_{B_i/I}, \dots, \boldsymbol{\omega}_{B_N/I}).$$
 19.

A word of caution regarding the notation is in order here. The meticulous reader will notice that in Equation 18, the state x is a collection of (regular) vectors that belong to \mathbb{R}^n and dual quaternions that are elements of \mathbb{H}_d . We make the tacit assumption here that dual quaternions can be replaced by their corresponding components in \mathbb{R}^8 using the standard bijection between \mathbb{H}_d and \mathbb{R}^8 as needed. In what follows, we make this correspondence implicit to avoid the introduction of additional bijection operators between \mathbb{R}^8 and \mathbb{H}_d that would only clutter the notation.

4.2. Dynamics

The dynamic equations can be easily derived by applying the Newton–Euler equations in terms of dual quaternions, that is, by computing the dual accelerations for each body and by applying the combined forces and moments acting on it. The latter can be combined together to form a dual wrench. A dual wrench (see the sidebar titled Dual Wrenches along with **Table 4**) is a dual quaternion where the real part is the force acting on the body and the dual part is the torque acting on the body about its center of mass. For joints, the balance of dual wrenches assumes that the reference point is the center of the joint (the origin of the corresponding joint frame; see

DUAL WRENCHES

Dual wrenches represent a combination of both the forces and torques acting on a body. For instance, if \bar{f}^{B_i} is the force and $\bar{\tau}^{B_i}$ is the torque about point O_{B_i} , in body B_i -frame coordinates, then $W_{B_i}(O_{B_i}) = f^{B_i} + \epsilon \tau^{B_i}$ denotes the dual body wrench, where $f^{B_i} = (0, \bar{f}^{B_i})$ and $\tau^{B_i} = (0, \bar{\tau}^{B_i})$. Similarly, the SMRS contains reaction wrenches, $W_{B_{i+1}/B_i}(O_{J_i})$, and actuation wrenches, $W_{J_i,\text{act}}(O_{J_i})$, at point O_{J_i} , expressed in J_i -frame coordinates. These wrenches constrain and actuate, respectively, the movement between bodies B_i and B_{i+1} . **Table 4** summarizes the various types of SMRS wrenches.

Table 4 Types of wrenches in spacecraft-mounted robotic systems

Joint type	$W_{ m J_j,act}$	$W^{\mathrm{J_{j}}}_{\mathrm{B_{i+1}/B_{i}}}$
Revolute	$(0, [0, 0, 0]^{T}) + \epsilon(0, [0, 0, \tau_z]^{T})$	$(0, [f_x, f_y, f_z]^{T}) + \epsilon(0, [\tau_x, \tau_y, 0]^{T})$
Prismatic	$(0, [0, 0, f_z]^{T}) + \epsilon(0, [0, 0, 0]^{T})$	$(0, [f_x, f_y, 0]^{T}) + \epsilon(0, [\tau_x, \tau_y, \tau_z]^{T})$
Spherical	$(0, [0, 0, 0]^{T}) + \epsilon(0, [\tau_x, \tau_y, \tau_z]^{T})$	$(0, [f_x, f_y, f_z]^{T}) + \epsilon(0, [0, 0, 0]^{T})$
Cylindrical	$(0, [0, 0, f_z]^{T}) + \epsilon(0, [0, 0, \tau_z]^{T})$	$(0, [f_x, f_y, 0]^{T}) + \epsilon(0, [\tau_x, \tau_y, 0]^{T})$
Cartesian	$(0, [f_x, f_y, f_z]^{T}) + \epsilon(0, [0, 0, 0]^{T})$	$(0,[0,0,0]^{T}) + \epsilon(0,[\tau_x,\tau_y,\tau_z]^{T})$
Actuation type	$W_{ m B_i,act}$	
Six-DOF	$(0, [f_x, f_y, f_z]^{T}) + \epsilon(0, [\tau_x, \tau_y, \tau_z]^{T})$	

Abbreviation: DOF, degree of freedom.

Figure 2). The development of the equations used to describe the multibody dynamics of an SMRS in this section is based on References 60–62.

The Newton-Euler equations of motion for a single rigid body in six-DOF motion are given as (63)

$$M_{\mathrm{B}_{\mathrm{i}}} \star \dot{\boldsymbol{\omega}}_{\mathrm{B}_{\mathrm{i}}/\mathrm{I}} + \boldsymbol{\omega}_{\mathrm{B}_{\mathrm{i}}/\mathrm{I}} \times \left(M_{\mathrm{B}_{\mathrm{i}}} \star \boldsymbol{\omega}_{\mathrm{B}_{\mathrm{i}}/\mathrm{I}} \right) = \boldsymbol{W}_{\mathrm{B}_{\mathrm{i}},\mathrm{sum}}(O_{\mathrm{B}_{\mathrm{i}}}),$$
 20.

where $W_{B_i,\text{sum}}(O_{B_i}) = f^{B_i} + \epsilon \tau^{B_i}$ is the sum of the total dual wrench applied on the B_i -th body about its center of mass, and the dual acceleration in the body frame is given by

$$\dot{\boldsymbol{\omega}}_{B_{i}/I} = \dot{\omega}_{B_{i}/I} + \epsilon \left(\dot{v}_{B_{i}/I} + \omega_{B_{i}/I} \times v_{B_{i}/I} \right).$$
 21.

In Equation 20, $M_{\rm B_i} \in \mathbb{R}^{8\times 8}$ denotes the dual inertia matrix of the B_i-th body, defined by

$$M_{\mathrm{B}_{\mathrm{i}}} \triangleq \begin{bmatrix} 0 & 0_{1\times3} & 1 & 0_{1\times3} \\ 0_{3\times1} & 0_{3\times3} & 0_{3\times1} & m_{\mathrm{B}_{\mathrm{i}}}I_{3\times3} \\ 1 & 0_{1\times3} & 0 & 0_{1\times3} \\ 0_{3\times1} & \bar{I}_{\mathrm{B}_{\mathrm{i}}} & 0_{3\times1} & 0_{3\times3} \end{bmatrix},$$
22.

where $m_{\rm B_i}$ is the mass of the B_i-th body, $\bar{I}_{\rm B_i} \in \mathbb{R}^{3\times3}$ is the mass inertia matrix of the B_i-th body, and $I_{3\times3}$ denotes the 3-by-3 identity matrix. The operator \star between a matrix $M \in \mathbb{R}^{8\times8}$ and a dual quaternion $\boldsymbol{a} = a_{\rm r} + \epsilon a_{\rm d}$ is defined as the dual quaternion (61, 63)

$$M \star a = (M_{11} * a_r + M_{12} * a_d) + \epsilon (M_{21} * a_r + M_{22} * a_d),$$
 23.

where $M_{11}, M_{12}, M_{21}, M_{22} \in \mathbb{R}^{4 \times 4}$ are the conformal subblocks of M and * denotes matrix/ quaternion multiplication (see **Table 1**).

To derive the dynamics for the N-body SMRS, we expand the total dual wrench $W_{B_i,sum}(O_{B_i})$, given in Equation 20 for a single body, to the various dual wrenches acting on the SMRS. **Figure 2** shows three types of dual wrenches. Specifically, the reaction and joint actuation wrenches appear at the joint, with their point of application being the origin of the joint frame O_{J_i} and their coordinates expressed in the J_i frame. The joint actuation wrenches $W_{J_i,act}(O_{J_i})$ induce motion about the DOFs of the joint, while the reaction wrenches $W_{B_{i+1}/B_i}(O_{J_i})$ arise due to physical constraints at the joints, and they are dual in nature to the joint actuation wrenches. Body wrenches, denoted as $W_{B_i}(O_{B_i})$, are assumed to act at the center of mass of the body B_i and arise due to control inputs (i.e., thrusters or momentum-exchange devices) or other natural sources (gravitational effects, atmospheric drag, solar pressure, etc.), all appropriately transformed to the center of mass through the shifting law.

Applying Equation 20 to the B_i-th body of the SMRS and expanding the right-hand side of the equation yields

$$M_{\mathrm{B},\star} \dot{\boldsymbol{\omega}}_{\mathrm{B},\mathrm{I}} + \boldsymbol{\omega}_{\mathrm{B},\mathrm{I}} \times (M_{\mathrm{B},\star} \star \boldsymbol{\omega}_{\mathrm{B},\mathrm{I}}) = \boldsymbol{W}_{\mathrm{B},\mathrm{I}}(O_{\mathrm{B},\mathrm{I}})$$
 24.

$$+\sum_{i=1}^{N-1} C_{ij} \boldsymbol{q}_{J_{j}/B_{i}} \left(\boldsymbol{W}_{J_{j},act}(O_{J_{j}}) + \boldsymbol{W}_{B_{i+1}/B_{i}}^{J_{j}}(O_{J_{j}}) + \boldsymbol{W}_{B_{i}/B_{i-1}}^{J_{j}}(O_{J_{j}}) \right) \boldsymbol{q}_{J_{j}/B_{i}}^{*},$$

where the components of the adjacency matrix are used to determine the correct signs of the respective reaction and actuation wrenches.

Now let \mathcal{T} denote the collection of all dual reaction wrenches between respective bodies as

$$\mathcal{T} = (W_{B_2/B_1}^{J_1}(O_{J_1}) \cdots W_{B_{i+1}/B_i}^{J_j}(O_{J_j}) \cdots W_{B_N/B_{N-1}}^{J_{N-1}}(O_{J_{N-1}})).$$
 25.

Collecting and rearranging Equation 24 for each body and using \mathcal{T} from Equation 25, we can summarize the equations of the SMRS in the following compact form:

$$\begin{bmatrix} \mathcal{S}_{11} & \mathcal{S}_{12} \\ \mathcal{S}_{21} & 0 \end{bmatrix} \star \begin{bmatrix} \dot{\boldsymbol{v}} \\ \mathcal{T} \end{bmatrix} = \begin{bmatrix} \mathcal{B}_1 \\ \mathcal{B}_2 \end{bmatrix},$$
 26.

where $S_{11} = \text{blkdiag}(M_{B_1} \cdots M_{B_i} \cdots M_{B_N})$ consists of the dual inertia matrix for each of the bodies, and where S_{12} and S_{21} contain the coordinate transformations of the unknown reaction wrenches that appear in the Newton–Euler form of the equations and the dual accelerations of each body from the constraint equations, respectively. (For the details of the construction of S_{21} and S_{12} in Equation 26, see Reference 61.)

The vector \mathcal{B}_1 is composed of a collection of subvectors, one for each B_i -th body, given by

$$(\mathcal{B}_{1})_{i} = -\boldsymbol{\omega}_{B_{i}/I} \times (M_{B_{i}} \star \boldsymbol{\omega}_{B_{i}/I}) + \boldsymbol{W}_{B_{i}}(O_{B_{i}}) + \sum_{j=1}^{N-1} C_{ij} \boldsymbol{q}_{J_{j}/B_{i}} \boldsymbol{W}_{J_{j},act}(O_{J_{j}}) \boldsymbol{q}_{J_{j}/B_{i}}^{*}.$$
 27.

The vector \mathcal{B}_2 corresponds to the right-hand side of the kinematic constraint equations for each of the J_i joints, where

$$(\mathcal{B}_2)_{i} = \mathbf{q}_{I:/B:}^* \boldsymbol{\omega}_{B_i/I} \mathbf{q}_{J_i/B_i} \times \boldsymbol{\omega}_{J_i/B_i}.$$
 28.

Given Equation 26, it follows that

$$\dot{\boldsymbol{v}} = \mathcal{S}_{11}^{-1} \star (\mathcal{B}_1 - \mathcal{S}_{12} \star \mathcal{T}), \tag{29}$$

where

$$\mathcal{T} = \left(S_{21}S_{11}^{-1}S_{12}\right)^{-1} \star \left(S_{21}S_{11}^{-1} \star \mathcal{B}_1 - \mathcal{B}_2\right).$$
 30.

Solving for the dual accelerations \dot{v} in Equation 29 allows for the construction of the derivative of $\dot{\Gamma}$ from Equation 17, which leads to

$$\ddot{\Gamma}_{j} = \dot{\Pi}_{j} \circledast \boldsymbol{\omega}_{J_{j}/B_{j}} + \Pi_{j} \circledast \dot{\boldsymbol{\omega}}_{J_{j}/B_{j}}, \qquad 31.$$

where, by making use of Equation 16, $\dot{\omega}_{J_i/B_i}$ is given as

$$\dot{\boldsymbol{\omega}}_{J_{j}/B_{i}} = \boldsymbol{q}_{B_{i+1}/J_{j}} \dot{\boldsymbol{\omega}}_{B_{i+1}/I} \boldsymbol{q}_{B_{i+1}/J_{i}}^{*} - \boldsymbol{q}_{J_{i}/B_{i}}^{*} \left(\dot{\boldsymbol{\omega}}_{B_{i}/I} + \boldsymbol{\omega}_{B_{i}/I} \times \boldsymbol{\omega}_{J_{i}/B_{i}}^{B_{i}} \right) \boldsymbol{q}_{J_{j}/B_{i}}.$$
32.

Finally, given Equations 14, 17, 29, and 32, we can express the time derivative of the system state x in Equation 18 as

$$\dot{\mathbf{x}} \triangleq (\dot{\mathbf{q}}_{\mathrm{B}_{1}/\mathrm{I}}, \dot{\Gamma}, \dot{\boldsymbol{\omega}}_{\mathrm{B}_{1}/\mathrm{I}}, \ddot{\Gamma}).$$
 33.

This equation can be integrated forward in time to generate the predicted SMRS motions. Note that for the purpose of control design, we may define the control inputs as

$$\boldsymbol{u} = (\boldsymbol{W}_{B_1,act}(O_{B_1}), \boldsymbol{W}_{J_1,act}(O_{J_1}), \dots \boldsymbol{W}_{J_{N-1},act}(O_{J_{N-1}})),$$
 34.

such that, by substituting \mathcal{T} from Equation 30 into Equation 29, we can write the dynamics of the SMRS as

$$\dot{\boldsymbol{v}} = \Phi(\mathbf{X}) + \Psi(\mathbf{X}) \star \boldsymbol{u}, \tag{35}$$

where $\Phi(\mathbf{x})$ is given by

$$\Phi(\mathbf{x}) = \mathcal{S}_{11}^{-1} (I_{8\times8} - \mathcal{S}_{12} (\mathcal{S}_{21} \mathcal{S}_{11}^{-1} \mathcal{S}_{12})^{-1} \mathcal{S}_{21} \mathcal{S}_{11}^{-1}) \star \mathcal{B}_{1,\text{nonact}}
+ \mathcal{S}_{11}^{-1} \mathcal{S}_{12} (\mathcal{S}_{21} \mathcal{S}_{11}^{-1} \mathcal{S}_{12})^{-1} \star \mathcal{B}_{2},$$
36.

with $(\mathcal{B}_{1,\text{nonact}})_i = -\boldsymbol{\omega}_{B_i/I} \times (M_{B_i} \star \boldsymbol{\omega}_{B_i/I}) + \boldsymbol{W}_{B_i}(O_{B_i})$, and $\Psi(\mathbf{x})$ is given by

$$\Psi(\mathbf{X}) = \mathcal{S}_{11}^{-1} (I_{8\times8} - \mathcal{S}_{12} (\mathcal{S}_{21} \mathcal{S}_{11}^{-1} \mathcal{S}_{12})^{-1} \mathcal{S}_{21} \mathcal{S}_{11}^{-1}) \mathcal{B}_{u},$$
 37.

where \mathcal{B}_u is a matrix composed of coordinate transformations related to \mathbf{q}_{J_j/B_i} and \mathbf{q}_{B_{i+1}/J_j} such that the actuation wrenches given by \mathbf{u} in Equation 34 are consistent with the dual accelerations of the bodies given in Equation 29.

5. PLANNING AND CONTROL

The operation of a robotic arm on a spacecraft is not a trivial task. Without appropriate dynamical models of the combined system and effective control algorithms, fuel can be quickly depleted, reaction wheels can saturate, power may be drawn too abruptly, a line-of-sight communication link may be lost, or the combined system can be destabilized. However, powerful techniques now exist that allow the base to move freely, or in a reactionless fashion, during the manipulation of the arm, thus avoiding the aforementioned pitfalls of a free-floating robotic manipulator. Masutani et al. (64) highlighted the fact that current algorithms must be able to incorporate changes, such as when a payload is released or grabbed or when there is a significant change in the fuel at the base. Another important component of the control problem is the incorporation of constraints beyond simple inertial pointing, as in the case of relative attitude constraints between spacecraft to avoid plume impingement, line-of-sight constraints to perform visual navigation, or simple obstacle avoidance constraints to avoid collision between satellites. The design of a servicing SMRS maneuver should also take into account uncertainties, which might be due to inaccurately modeled effects such as flexibility and fuel sloshing, poor characterization of the object manipulated by the end effector, or external disturbances typical of the space environment (solar radiation pressure, magnetic field, etc.); hence, adaptive or robust control techniques might be needed.

Similarly to the modeling aspects of an SMRS, planning and control can be categorized according to whether the satellite base is actively controlled or not. In the first case, a coordinated control strategy (42, 65, 66) is adopted in order to stabilize the position and/or attitude of the satellite base during the maneuvering phase of the robotic appendages; a greater importance is therefore attributed to the satellite stabilization performance (67), fuel- or energy-efficient control strategies (68), or possible actuation limits (69).

Internal control methods (20, 47, 70), by contrast, consider an unactuated base, and hence must account for the spacecraft displacement while planning the motion of the manipulator. This translates into a more complex control architecture, which nevertheless has the advantage of saving fuel and power.

5.1. The Free-Flying Case

In the free-flying case, the center of mass of the system can be displaced, resulting in greater flexibility and a larger workspace. The downside is that thruster firing depletes fuel, a rare commodity in space. So, ideally, a free-flying SMRS should factor in the impact of the planned maneuver on fuel consumption.

Dubowsky et al. (39) addressed the problem of thruster and joint actuator saturation as an integral part of the manipulator path-planning problem. They argued that for fixed-base manipulators much of the literature has focused on minimum-time path planning; however, greater manipulator speeds result in larger disturbances. Lampariello et al. (71) formulated the free-flyer's path-planning problem from an optimal guidance perspective, seeking to minimize the control effort necessary to stabilize the satellite throughout the maneuver. The problem is constrained by mission goals (the position and orientation of the end effector at the final time) along with kinematic and dynamic constraints, such as joint limits and saturation of the actuators. The position and orientation variables are parameterized with respect to time as quintic polynomials, and the resulting optimization problem is solved through sequential quadratic programming. As expected, when the goal pose is in the local workspace of the robot, the optimal plan comes down to a freefloating maneuver, since the base does not need to be actuated to reach the desired end-effector configuration. Jacobsen & Zhu (72) presented a numerical optimization framework for the design of a kinematic trajectory to grasp an uncontrolled spinning target. They defined the cost function mainly on the basis of safety considerations and tried to maximize the time to collision in the event of a loss of power of the chaser spacecraft. Fuel usage, the length of the maneuver, and actuator constraints were also taken into consideration. The optimized path was compared with a heuristically defined one, and the authors proved that the former strikes a better balance among safety, fuel consumption, and total maneuvering time.

The nonlinear nature of the free-flying SMRS dynamics is particularly evident when the spacecraft-mounted robot executes fast maneuvers, which, for instance, may bring about flexibility effects or induce fuel sloshing. As a consequence, numerous nonlinear control approaches have been investigated by the community to remedy these effects. Senda et al. (67) derived and tested two nonlinear controllers, using control moment gyros to regulate the attitude of the base: a Lyapunov-type controller that included an integral term for disturbance rejection and an exact input–output feedback linearization. When comparing the two approaches, the authors highlighted that the latter leads to an easier design procedure. Chen & Meirovitch (73) coped with flexible nonlinear dynamics in the context of a tracking/docking maneuver by means of two different components: a Lyapunov-like online feedback tracking controller and a discrete-time linear–quadratic regulator for vibration suppression.

A common limitation of the aforementioned studies is that they implicitly assume exact knowledge of the system. Adaptive and robust methods remove such underlying assumptions and tackle

uncertainties within the same control framework. Among the many available studies, Grewal & Modi (74) illustrated the advantages deriving from the application of robust control techniques such as linear–quadratic–Gaussian/loop transfer recovery (LQG/LTR) and H_{∞} to the control of a large, flexible space structure with appendages. Both controllers achieve satisfactory stabilization of the attitude motion, and the authors argued that the H_{∞} control approach, due to its nature, requires fewer design iterations than the LQG/LTR approach in order to achieve the desired shape of the closed-loop transfer function. Walker & Wee (75) presented a passivity-based adaptive tracking controller that meets the global asymptotic convergence condition presented by Ortega & Spong (76). Even in the absence of any estimates of the inertial parameters or of the initial momentum, the proposed method achieves good tracking performance of a second-order polynomial trajectory. The well-known Slotine–Li regressor matrix (77), originally developed in the context of ground-fixed payload manipulation, was revisited by Senda et al. (78) and adapted to the case of a stabilized spacecraft grasping an unknown payload with a robotic arm. The stability of the closed-loop system, including both satellite and manipulator variables, was proved through Lyapunov's second method.

5.2. The Free-Floating Case

For reasons outlined above, most of the literature in controlling SMRSs has been devoted to the free-floating case. However, the development of the equations of motion in this case is not as straightforward as it is in the free-flying case, due to the complex interaction between reaction forces that arise at the joints and the conservation-of-momentum constraints.

One of the most interesting works in this vein was by Umetani & Yoshida (47), who introduced the equations of motion for SMRSs with revolute joints and an uncontrolled base. Their formulation would become a landmark due to the introduction of the generalized Jacobian matrix and its utilization for solving the inverse kinematics for the generalized velocities that achieve a desired end-effector motion. Their approach allows for precise control of the end effector with minimal or zero fuel usage when the trajectory is in the workspace of the robot. The authors also highlighted the difficulty of studying the kinematics of a robotic arm on a free base. Specifically, since the pose is generally history dependent, it is preferable to work with the rates of change of the configuration variables instead of attempting to control their actual values.

In a later publication, Masutani et al. (64) made use of the generalized Jacobian matrix by proposing a control law that achieves asymptotic stabilization of the end-effector position and attitude. However, the approach holds only for a time-invariant desired pose, and the result is local, as conditions on the linear and angular parts of the generalized Jacobian matrix are imposed from the outset. In a follow-up work (79), the same authors analyzed a linearized version of the dynamics and showed that the performance of the controller when the generalized Jacobian matrix is substituted for the conventional Jacobian is much less computationally intensive and improves with the ratio of masses of the base and the arm. Xu & Shum (6) also adopted the generalized Jacobian matrix to characterize the motion of the end effector in the absence of thruster jets as a function of the generalized joint states and those of the base. Caccavale & Siciliano (80) made use of the generalized Jacobian and adopted quaternions for attitude representation of the base. They proposed a joint velocity control law that uses the vector part of the quaternion error as feedback, even though this quaternion is computed from the product of rotation matrices.

For free-floating scenarios, even though the linear and angular momentum conservation equations are a function of the velocities, the linear conservation of momentum is simply a function of the center-of-mass location. Nakamura & Mukherjee (81) emphasized this fact and introduced the use of nonholonomicity in the analysis of the equations of motion. This work made use of the

nonholonomic constraints to control the attitude of the satellite using only the motion of the joints. The approach uses the generalized velocities of the joints and Lyapunov's direct method to avoid neglecting higher-order terms, as was done by Vafa & Dubowsky (49). In a later work, Nakamura & Mukherjee (82) delved more deeply into formalizing the analysis of the holonomicity of a space robot and introduced the bidirectional approach, which consists of having a virtual robot with the same dynamics whose initial condition is the desired state. Through the design of an appropriate control input for both systems, if the error dynamics of these robotic arms converges to zero, then the actual control is just a reflection of the virtual system's control input reflected and shifted in the time domain. Although the authors claimed that the proposed bidirectional approach ameliorates their previous results (81), global asymptotic stability of the proposed controller is still not guaranteed.

A meaningful distinction in the free-floating literature exists between studies that assume null initial momentum and those that do not. The second case accounts for scenarios when momentum is accumulated throughout the maneuver (due to, e.g., the contact of the robot with an external object), hence originating a persisting excitation acting on the system. This has the effect of causing a deviation of the end effector (83, 84). Papadopoulos & Dubowsky (85) assumed zero initial angular momentum in order to obtain a compact representation of the kinetic energy of the system and to derive the dynamic equations in a Lagrangian fashion. They proceeded to argue that fixed-base and space-based manipulators can, in theory, almost always be controlled using the same control algorithms, given the structural similarities between the model matrices. However, the free-floating Jacobian depends on the attitude of the base, and the inertia matrix is a function of the spacecraft's mass properties. Therefore, satisfactory performance of control laws derived for ground-fixed platforms remains subject to an accurate characterization of the free-floating system.

When a control algorithm is applied to the free-floating case, it also must be able to overcome dynamic singularities, which do not arise in the fixed-base case. The problem of path planning while avoiding dynamic singularities was tackled by Nanos & Papadopoulos (86) under the assumption of zero initial momentum. The authors characterized the dynamically singular surfaces in the configuration space and found the initial orientation of the spacecraft, which allows the system to never encounter a singularity while moving along the desired trajectory. In a later work (87), they generalized this approach by removing the assumption of zero angular momentum.

The problem of establishing the controllability and stabilizability of a planar multibody system in space under the assumption of zero angular momentum was thoroughly investigated by Reyhanoglu & McClamroch (88, 89). They showed that the linearization of the system is inconclusive for the purpose of studying controllability, and they therefore resorted to specific results from nonlinear control theory, such as accessibility and small-time local controllability (90). They argued that, once small-time local controllability has been shown, asymptotic stabilization cannot be obtained through a smooth feedback control law, and they therefore constructed a discontinuous feedback controller that successfully stabilizes the system's origin.

Nonzero angular momentum was investigated, for example, by Nanos & Papadopoulos (83), who proposed a framework that allows the end effector to be kept fixed in space. The authors later extended these initial results to include general Cartesian or joint-space tracking (91).

5.3. A Dual Quaternion Spacecraft-Mounted Robotic System Pose-Tracking Controller

As an example of the usefulness of the modeling approach based on dual quaternions (described in Section 4.2), in this section we illustrate a control design for tracking the pose of both the spacecraft base and the end effector of a free-flying SMRS.

Let G denote the frame of the end effector, and consider the pose of the end effector of an SMRS given by the kinematic relationship

$$q_{G/I} = q_{B_1/I}q_{J_i/B_i}q_{B_{i+1}/J_i}\dots q_{J_{N-1}/B_{N-1}}q_{B_N/J_{N-1}}q_{G/B_N},$$
38.

as well as the end effector's dual velocity, $\boldsymbol{\omega}_{G/I} = \boldsymbol{q}_{G/B_N}^* \boldsymbol{\omega}_{B_N/I} \boldsymbol{q}_{G/B_N}$, and dual acceleration, $\dot{\boldsymbol{\omega}}_{G/I} = \boldsymbol{q}_{G/B_N}^* \dot{\boldsymbol{\omega}}_{B_N/I} \boldsymbol{q}_{G/B_N}$. Given two desired time-varying reference frames, one for the end effector (denoted by E) and one for the base of the spacecraft (denoted by S), we can express the corresponding relative error poses as $\boldsymbol{q}_{G/E} = \boldsymbol{q}_{E/I}^* \boldsymbol{q}_{G/I}$ and $\boldsymbol{q}_{B_1/S} = \boldsymbol{q}_{S/I}^* \boldsymbol{q}_{B_1/I}$. Thus, the relative kinematics between the desired frames of the SMRS base and end effector evolve, respectively, as

$$\dot{\boldsymbol{q}}_{\mathrm{G/E}} = \frac{1}{2} \boldsymbol{q}_{\mathrm{G/E}} \boldsymbol{\omega}_{\mathrm{G/E}} \quad \text{and} \quad \dot{\boldsymbol{q}}_{\mathrm{B}_{1}/\mathrm{S}} = \frac{1}{2} \boldsymbol{q}_{\mathrm{B}_{1}/\mathrm{S}} \boldsymbol{\omega}_{\mathrm{B}_{1}/\mathrm{S}},$$
 39.

where $\boldsymbol{\omega}_{G/E} = \boldsymbol{\omega}_{G/I} - \boldsymbol{\omega}_{E/I}^G$ and $\boldsymbol{\omega}_{B_1/S} = \boldsymbol{\omega}_{B_1/I} - \boldsymbol{\omega}_{S/I}^{B_1}$.

We can, additionally, express the relative dual acceleration of the end effector and the satellite base with respect to the desired reference frames E and S as $\dot{\boldsymbol{\omega}}_{G/E} = \dot{\boldsymbol{\omega}}_{G/I} - \dot{\boldsymbol{\omega}}_{E/I}^G$ and $\dot{\boldsymbol{\omega}}_{B_1/S} = \dot{\boldsymbol{\omega}}_{B_1/I} - \dot{\boldsymbol{\omega}}_{S/I}^{B_1}$, respectively. From the transport theorem (57), it follows that $\dot{\boldsymbol{\omega}}_{E/I}^G = \boldsymbol{q}_{G/E}^*(\dot{\boldsymbol{\omega}}_{E/I} - \boldsymbol{\omega}_{G/E}^E \times \boldsymbol{\omega}_{E/I}) \boldsymbol{q}_{G/E}$ and $\dot{\boldsymbol{\omega}}_{S/I}^{B_1} = \boldsymbol{q}_{B_1/S}^*(\dot{\boldsymbol{\omega}}_{S/I} - \boldsymbol{\omega}_{B_1/S}^S \times \boldsymbol{\omega}_{S/I}) \boldsymbol{q}_{B_1/S}$. Given the dynamics of each rigid body and the end effector of an SMRS as in Equation 35, we can express the spacecraft-base and end-effector dynamics as, respectively,

$$\dot{\boldsymbol{\omega}}_{B_1/I} = \Phi_1(\mathbf{x}) + \Psi_1(\mathbf{x}) \star \boldsymbol{u}_{B_1}, \tag{40}$$

$$\dot{\boldsymbol{\omega}}_{G/I} = \boldsymbol{q}_{G/B_N}^* \left(\Phi_N(\mathbf{X}) + \Psi_N(\mathbf{X}) \star \boldsymbol{u}_{J_1 \cdot N_{-1}} \right) \boldsymbol{q}_{G/B_N},$$
 41.

where u_{B_1} and $u_{J_{1:N-1}}$ are the wrenches generated from the spacecraft base and manipulator, respectively, such that $u = (u_{B_1}, u_{J_{1:N-1}})$.

Now let matrices K_{B_1} , $K_G > 0$ and scalars p_{B_1} , p_G , k_{B_1} , $k_G > 0$, and consider the following feedback control law:

 $\Psi_{1,N}(\mathbf{x}) \star \mathbf{u}$

$$= \left\{ \begin{aligned} &-\Phi_{1}(\mathbf{x}) + \dot{\boldsymbol{\omega}}_{\mathrm{S}/\mathrm{I}}^{\mathrm{B}_{1}} + \mathsf{S}(K_{\mathrm{B}_{1}}^{-1}) \star \left(-k_{\mathrm{B}_{1}} \boldsymbol{\omega}_{\mathrm{B}_{1}/\mathrm{S}} - p_{\mathrm{B}_{1}} \mathrm{vec} \left(\boldsymbol{q}_{\mathrm{B}_{1}/\mathrm{S}}^{*} \left(\boldsymbol{q}_{\mathrm{B}_{1}/\mathrm{S}} - 1 \right)^{\mathrm{s}} \right)^{\mathrm{s}} \right) \\ &-\Phi_{\mathrm{N}}(\mathbf{x}) + \boldsymbol{q}_{\mathrm{G}/\mathrm{B}_{\mathrm{N}}} \left(\dot{\boldsymbol{\omega}}_{\mathrm{E}/\mathrm{I}}^{\mathrm{G}} + \mathsf{S}(K_{\mathrm{G}}^{-1}) \star \left(-k_{\mathrm{G}} \boldsymbol{\omega}_{\mathrm{G}/\mathrm{E}} - p_{\mathrm{G}} \mathrm{vec} \left(\boldsymbol{q}_{\mathrm{G}/\mathrm{E}}^{*} \left(\boldsymbol{q}_{\mathrm{G}/\mathrm{E}} - 1 \right)^{\mathrm{s}} \right)^{\mathrm{s}} \right) \right) \boldsymbol{q}_{\mathrm{G}/\mathrm{B}_{\mathrm{N}}}^{*} \right\}, \end{aligned}$$

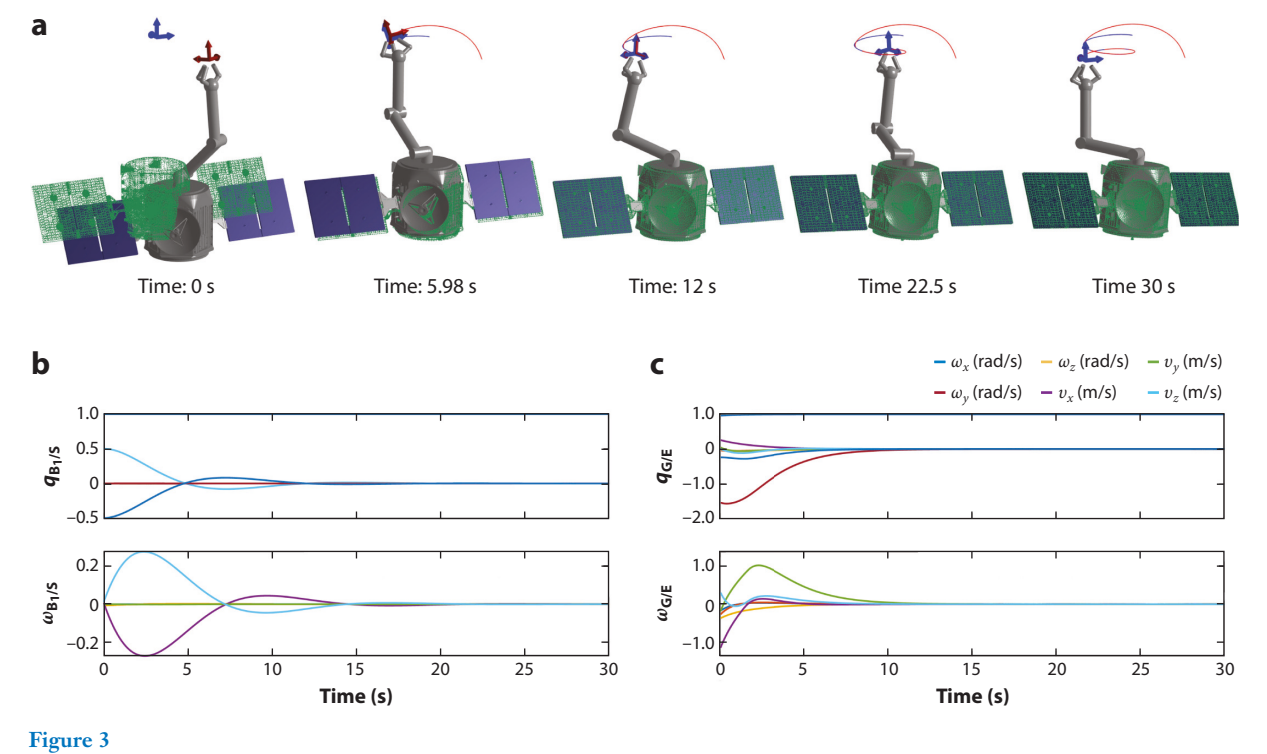
where $\Psi_{1,N}(\mathbf{x}) = [\Psi_1^{\mathsf{T}}(\mathbf{x}) \ \Psi_N^{\mathsf{T}}(\mathbf{x})]^{\mathsf{T}}$, and define $S(\cdot) : \mathbb{R}^{8 \times 8} \to \mathbb{R}^{8 \times 8}$ such that, if $\mathbf{a} \in \mathbb{H}_d$ and $T \in \mathbb{R}^{8 \times 8}$, then $(S(T) \star \mathbf{a})^{\mathsf{S}} = T \star (\mathbf{a})^{\mathsf{S}}$. This control law results in $\mathbf{q}_{B_1/S}(t) \to \pm 1$, $\mathbf{q}_{G/E}(t) \to \pm 1$, $\omega_{B_1/S}(t) \to 0$, and $\omega_{G/E}(t) \to 0$ as $t \to \infty$. To see this, it suffices to use the candidate Lyapunov function

$$V(\mathbf{q}_{B_{1}/S}, \mathbf{\omega}_{B_{1}/S} \mathbf{q}_{G/E}, \mathbf{\omega}_{G/E}) = \frac{1}{2} (\mathbf{\omega}_{B_{1}/S})^{s} \circ (K_{B_{1}} \star (\mathbf{\omega}_{B_{1}/S})^{s}) + p_{B_{1}} (\mathbf{q}_{B_{1}/S} - 1) \circ (\mathbf{q}_{B_{1}/S} - 1)$$
$$+ \frac{1}{2} (\mathbf{\omega}_{G/E})^{s} \circ (K_{G} \star (\mathbf{\omega}_{G/E})^{s}) + p_{G} (\mathbf{q}_{G/E} - 1) \circ (\mathbf{q}_{G/E} - 1). \quad 43.$$

It is straightforward to show that the time derivative of V when implementing the control law in Equation 42 is given as

$$\dot{V} = -k_{\mathrm{B}_{1}} \left(\boldsymbol{\omega}_{\mathrm{B}_{1}/\mathrm{S}} \right)^{\mathrm{S}} \circ \left(\boldsymbol{\omega}_{\mathrm{B}_{1}/\mathrm{S}} \right)^{\mathrm{S}} - k_{\mathrm{G}} \left(\boldsymbol{\omega}_{\mathrm{G}/\mathrm{E}} \right)^{\mathrm{S}} \circ \left(\boldsymbol{\omega}_{\mathrm{G}/\mathrm{E}} \right)^{\mathrm{S}} \leq 0, \tag{44}$$

guaranteeing that $q_{B_1/S}$, $\omega_{B_1/S}$, $q_{G/E}$, and $\omega_{G/E}$ are uniformly bounded. A signal-chasing argument, along with the use of Barbalat's lemma (92), yields $\omega_{B_1/S}(t) \to 0$ and $\omega_{G/E}(t) \to 0$, and also that



(a) RRRS spacecraft-mounted robotic system. (b) Relative dual quaternions and dual velocities of the RRRS spacecraft-mounted robotic system-base frame. (c) Relative dual quaternions and dual velocities of the RRRS spacecraft-mounted robotic system end-effector frame. Abbreviations: R, revolute; S, spherical.

 $q_{\rm B_1/S}(t) \to \pm 1$ and $q_{\rm G/E}(t) \to \pm 1$ as $t \to \infty$. Note that $q_{\rm B_1/S}=1$ and $q_{\rm B_1/S}=-1$ represent the same spacecraft-base poses and $q_{\rm G/E}=1$ and $q_{\rm G/E}=-1$ represent the same end-effector poses, and either equilibrium point is therefore acceptable. However, this can lead to the well-known unwinding phenomenon, where a large rotation (>180°) is performed even though a smaller rotation (<180°) exists. This can be resolved by switching the gains in Equation 42 in order to follow the shortest path to the equilibrium (93).

Figure 3 shows the relative dual quaternions and dual velocities between the spacecraft base B_1 with respect to the desired reference frame S (**Figure 3**b) and between the SMRS end-effector frame G and desired end-effector reference frame E (**Figure 3**c). It is seen that $q_{B_1/S}(t) \to 1$ and $\omega_{B_1/S}(t) \to 0$ and that $q_{G/E}(t) \to 1$ and $\omega_{G/E}(t) \to 0$ as $t \to \infty$.

6. CURRENT AND FUTURE OUTLOOK

Satellites are the unsung heroes of the digital age. They have transformed society by changing the way we conduct our work, the way we communicate with each other, and the way we monitor the environment. Unfortunately, currently, once a satellite malfunctions, there is very little that can be done to mitigate the failure. Space operators are therefore willing to accept high failure rates (~13%) as part of doing business in space (94), but no other industry would be willing to accept such high failure rates as normal. There is obviously a clear need for cost-effective servicing, health monitoring, and repair of highly valuable space assets in orbit. Furthermore, many planned missions to Mars and beyond also envision robotic assembly operation around the destination planet

orbit (95). Owing to the distances and environmental hazards involved, using humans alone is not a realistic option to perform these missions. Robotic spacecraft, perhaps working autonomously or alongside human astronauts, are well suited to fill this gap.

Recognizing these trends, NASA has recently identified robotic operations as a crucial technology that would enable a plethora of future missions in space (96). In fact, space robotics missions currently under planning, such as the On-Orbit Servicing, Assembly, and Manufacturing 1 (OSAM-1) mission, go beyond simply capturing resident space objects or performing minor servicing operations. The OSAM-1 spacecraft will perform refueling of Landsat 7, an Earth observation satellite that launched in 1999 and was never meant to be serviced. Moreover, OSAM-1 will assemble a functional 3-m communications antenna and manufacture a lightweight composite beam. In the future, the availability of robotic manipulators in space will open a slew of possibilities that include in-space assembly of large structures, payload transfer between orbiting satellites, in situ resource utilization, rescue missions of stranded touristic space vehicles, effective momentum transfer of a detumbling spacecraft, debris capture, and unmanned manipulation and disassembly of adversary satellites, just to name a few (97–99).

7. CONCLUSIONS

The modeling of SMRSs has evolved from merely a problem of academic interest to a problem that has immediate practical applications. Recent advances in the modeling and control of multibody systems, machine learning algorithms, and robotics system integration, along with the reduced cost of space access, have catapulted space robotics and space autonomy into a crucial role for many future space missions. A better understanding of the complex interaction of spacecraft robotic manipulators with the spacecraft base will allow more precise path planning and trajectory tracking for a wide range of applications in a computationally efficient manner.

SUMMARY POINTS

- Spacecraft-mounted robotic systems (SMRSs) are indispensable for future servicing missions in orbit.
- Depending on whether the spacecraft base is actuated, SMRSs can be classified as either free-flying or free-floating.
- Dual quaternions offer a compact description of the combined rotational and translational motion of SMRSs.
- The compact representation afforded by the use of dual quaternions results in easier control design.

FUTURE ISSUES

- Coordinated control of the spacecraft base and manipulator is necessary for highperformance SMRSs.
- 2. Future challenges include understanding and mitigating flexibility effects as well as integrating soft robotic mechanisms into SMRSs.
- Human–robot collaboration in orbit for manipulation tasks will introduce new challenges but also offer opportunities for new space servicing missions.

DISCLOSURE STATEMENT

The authors are not aware of any affiliations, memberships, funding, or financial holdings that might be perceived as affecting the objectivity of this review.

ACKNOWLEDGMENTS

The authors would like to thank Alfredo Valverde and Nuno Filipe for many helpful discussions. Support for this work has been provided by National Science Foundation awards NRI-1426945 and FRR-2101250, Air Force Research Laboratory award FA9453-13-C-0201, and a Jet Propulsion Laboratory Strategic University Research Partnership award.

LITERATURE CITED

- Wilde M, Harder J, Stoll E. 2019. Editorial: on-orbit servicing and active debris removal: enabling a paradigm shift in spaceflight. Front. Robot. AI 6:136
- Goddard Space Flight Cent. 2010. On-orbit satellite servicing study. Rep., Goddard Space Flight Cent., Natl. Aeronaut. Space Adm., Greenbelt, MD
- Reed BB. 2011. Robotic refueling mission overview. Presentation at the Future In-Space Operations Colloquium, Aug. 3
- Natl. Sci. Technol. Counc. 2022. In-space servicing, assembly, and manufacturing national strategy. Rep., Natl. Sci. Technol. Counc., Washington, DC. https://www.whitehouse.gov/wp-content/uploads/2022/04/04-2022-ISAM-National-Strategy-Final.pdf
- Akin DL. 2014. Innovative robotic systems for in-space operations. Presentation at the Future In-Space Operations Colloquium, Jan. 22. https://fiso.spiritastro.net/telecon13-15/Akin_1-22-14/Akin_1-22-14. pdf
- Xu Y, Shum HY. 1991. Dynamic control of a space robot system with no thrust jets controlled base. Tech. Rep. CMU-RI-TR-91-33, Robot. Inst., Carnegie Mellon Univ., Pittsburgh, PA
- Bronez MA, Clarke MM, Quinn A. 1986. Requirements development for a free-flying robot—the "Robin." In 1986 International Conference on Robotics and Automation (ICRA), pp. 667–72. Piscataway, NJ: IEEE
- Akin D, Misky ML, Thiel E, Kurtzman C. 1983. Space Applications of Automation, Robotics and Machine Intelligence Systems (ARAMIS) – Phase 2, Vol. 1: Telepresence Technology Base Development. Washington, DC: Natl. Aeronaut. Space Adm.
- Qu R, Takei Y, Oda M, Nakanishi H, Wedler A, Yoshikawa K. 2017. A study on the end-effector exchange mechanism of a space robot. J. Mech. Eng. Autom. 7:278–84
- Flores-Abad A, Ma O, Pham K, Ulrich S. 2014. A review of space robotics technologies for on-orbit servicing. Prog. Aerosp. Sci. 68:1–26
- Kassel S. 1971. Lunokhod-1 Soviet lunar surface vehicle. Tech. Rep. R-802-ARPA, RAND Corp., Santa Monica, CA. https://apps.dtic.mil/sti/pdfs/AD0733960.pdf
- Wilcox B, Nguyen T. 1998. Sojourner on Mars and lessons learned for future planetary rovers. Tech. Pap. 981695, SAE Int., Warrendale, PA
- Crisp JA, Adler M, Matijevic JR, Squyres SW, Arvidson RE, Kass DM. 2003. Mars Exploration Rover mission. 7. Geophys. Res. Planets 108:8061
- Grotzinger JP, Crisp J, Vasavada AR, Anderson RC, Baker CJ, et al. 2012. Mars Science Laboratory Mission and science investigation. Space Sci. Rev. 170:5–56
- Farley K, Williford K, Stack K, Bhartia R, Chen A, et al. 2020. Mars 2020 mission overview. Space Sci. Rev. 216:142
- 16. Ellery A. 2016. Planetary Rovers: Robotic Exploration of the Solar System. Berlin: Springer
- 17. Yoshida K. 2001. ETS-VII flight experiments for space robot dynamics and control. In *Experimental Robotics VII*, ed. D Rus, S Singh, pp. 209–18. Berlin: Springer

- Oda M. 1999. Space robot experiments on NASDA's ETS-VII satellite—preliminary overview of the experiment results. In 1999 International Conference on Robotics and Automation (ICRA), Vol. 2, pp. 1390–95. Piscataway. NI: IEEE
- Oda M. 2001. ETS-VII: achievements, troubles and future. In I-SAIRAS 2001: A New Space Odyssey; Proceedings of the 6th International Symposium on Artificial Intelligence, Robotics and Automation in Space. Longueuil, Can.: Can. Space Agency
- Umetani Y, Yoshida K. 1987. Continuous path control of space manipulators mounted on OMV. Acta Astronaut. 15:981–86
- Yoshida K, Nenchev DN, Uchiyama M. 1996. Moving base robotics and reaction management control. In *Robotics Research: The Seventh International Symposium*, ed. G Giralt, G Hirzinger, pp. 100–9. London: Springer
- Natl. Aeronaut. Space Adm. 2018. Remote manipulator system (Canadarm2). National Aeronautics and Space Administration. https://www.nasa.gov/mission_pages/station/structure/elements/remote-manipulator-system-canadarm2
- Matsueda T, Kuraoka K, Goma K, Sumi T, Okamura R. 1991. JEMRMS system design and development status. In NTC '91 – National Telesystems Conference Proceedings, pp. 391–95. Piscataway, NJ: IEEE
- Boumans R, Heemskerk C. 1998. The European Robotic Arm for the International Space Station. Robot. Auton. Syst. 23:17–27
- Hirzinger G, Brunner B, Dietrich J, Heindl J. 1994. ROTEX—the first remotely controlled robot in space. In *Proceedings of the 1994 IEEE International Conference on Robotics and Automation (ICRA)*, Vol. 3, pp. 2604–11. Piscataway, NJ: IEEE
- Hirzinger G, Landzettel K, Reintsema D, Preusche C, Albu-Schaffer A, et al. 2005. ROKVISS—robotics
 component verification on ISS. In Proceedings of i-SAIRAS 2005: The 8th International Symposium on
 Artificial Intelligence, Robotics and Automation in Space. Noordwijk, Neth.: ESA Publ. Div.
- Shoemaker J, Wright M. 2004. Orbital express space operations architecture program. In Spacecraft Platforms and Infrastructure, ed. P Tchoryk Jr., M Wright, pp. 57–65. Bellingham, WA: SPIE
- Henshaw CG. 2009. NRL robotics overview. Presentation to the Future In-Space Operations Colloquium, July 29. https://fiso.spiritastro.net/telecon07-09/Henshaw_7-29-09/Henshaw%20FREND% 20Overview%207_29_09.pdf
- Roesler G. 2016. Robotic Servicing of Geosynchronous Satellites (RSGS) program overview. Presentation to the Future In-Space Operations Colloquium, June 15. http://images.spaceref.com/fiso/2016/061516_ roesler_darpa/Roesler_6-15-16.pdf
- Reed BB. 2017. NASA satellite servicing evolution. Presentation to the Future In-Space Operations Colloquium, Jan. 11. http://images.spaceref.com/fiso/2017/011117_reed/Reed_1-11-17.pdf
- Barnhart D, Sullivan B, Hunter R, Bruhn J, Fowler E, et al. 2013. Phoenix Program Status 2013. In AIAA SPACE Conference and Exposition, pap. 2013-5341. Reston, VA: Am. Inst. Aeronaut. Astronaut.
- Spacefl. 101. 2016. China's new orbital debris clean-up satellite raises space militarization concerns. *Spaceflight101*, June 29. https://spaceflight101.com/long-march-7-maiden-launch/aolong-1-asat-concerns
- Brophy JR, Friedman L, Culick F. 2012. Asteroid retrieval feasibility. In 2012 IEEE Aerospace Conference. Piscataway, NJ: IEEE. https://www.kiss.caltech.edu/papers/asteroid/papers/asteroid_retrieval.pdf
- Strange N, Landau D, McElrath T, Lantoine G, Lam T, et al. 2013. Overview of mission design for NASA Asteroid Redirect Robotic Mission concept. In 33rd International Electric Propulsion Conference, pap. 2013-321. Pasadena, CA: Jet Propuls. Lab.
- Reuter GJ, Hess CW, Rhoades DE, McFadin LW, Healey KJ, Erickson JD. 1988. An intelligent, freeflying robot. In Space Station Automation IV, ed. WC Chiou Sr., pp. 20–27. Bellingham, WA: SPIE
- Moosavian SAA, Papadopoulos E. 2004. Explicit dynamics of space free-flyers with multiple manipulators via SPACEMAPLE. Adv. Robot. 18:223

 –44
- Moosavian SAA, Papadopoulos E. 1998. On the kinematics of multiple manipulator space free-flyers and their computation. J. Robot. Syst. 15:207–16
- Papadopoulos E. 1991. On the dynamics and control of space manipulators. PhD Thesis, Mass. Inst. Technol., Cambridge, MA

- Dubowsky S, Vance EE, Torres MA. 1989. The control of space manipulators subject to spacecraft attitude control saturation limits. In *Proceedings of the NASA Conference on Space Telerobotics*, Vol. 4, pp. 409–18. Pasadena, CA: Jet Propuls. Lab.
- Egeland O, Sagli JR. 1993. Coordination of motion in a spacecraft/manipulator system. Int. J. Robot. Res. 12:366–79
- Luh JY, Walker MW, Paul RP. 1980. On-line computational scheme for mechanical manipulators. J. Dyn. Syst. Meas. Control 102:69–76
- Carignan CR, Akin DL. 2000. The reaction stabilization of on-orbit robots. IEEE Control Syst. Mag. 20(6):19–33
- 43. Featherstone R. 2008. Rigid Body Dynamics Algorithms. Berlin: Springer
- Nenchev DN, Yoshida K. 1999. Impact analysis and post-impact motion control issues of a free-floating space robot subject to a force impulse. IEEE Trans. Robot. Autom. 15:548–57
- Seddaoui A, Saaj CM. 2019. Combined nonlinear b_∞ controller for a controlled-floating space robot.
 Guid. Control Dyn. 42:1878–85
- Seddaoui A, Saaj CM, Nair MH. 2021. Modeling a controlled-floating space robot for in-space services: a beginner's tutorial. Front. Robot. AI 8:725333
- Umetani Y, Yoshida K. 1989. Resolved motion rate control of space manipulators with generalized Jacobian matrix. *IEEE Trans. Robot. Autom.* 5:303–14
- Papadopoulos E, Dubowsky S. 1993. Dynamic singularities in free-floating space manipulators. J. Dyn. Syst. Meas. Control 115:44–52
- Vafa Z, Dubowsky S. 1987. On the dynamics of manipulators in space using the virtual manipulator approach. In 1987 IEEE International Conference on Robotics and Automation (ICRA), pp. 579

 –85. Piscataway, NJ: IEEE
- Vafa Z, Dubowsky S. 1990. The kinematics and dynamics of space manipulators: the virtual manipulator approach. Int. J. Robot. Res. 9:3–21
- Vafa Z, Dubowsky S. 1990. On the dynamics of space manipulators using the virtual manipulator, with applications to path planning. J. Astronaut. Sci. 38:441–72
- 52. Vafa Z, Dubowsky S. 1993. On the dynamics of space manipulators using the virtual manipulator, with applications to path planning. In *Space Robotics: Dynamics and Control*, ed. Y Xu, T Kanade, pp. 45–76. Boston: Springer
- 53. Longman R. 1993. The kinetics and workspace of a satellite-mounted robot. In *Space Robotics: Dynamics and Control*, ed. Y Xu, T Kanade, pp. 27–44. Boston: Springer
- Dubowsky S, Torres MA. 1991. Path planning for space manipulators to minimize spacecraft attitude disturbances. In 1991 IEEE International Conference on Robotics and Automation (ICRA), Vol. 3, pp. 2522–28. Piscataway, NJ: IEEE
- Perez A, McCarthy JM. 2004. Dual quaternion synthesis of constrained robotic systems. J. Mech. Des. 126:425–35
- Pham HL, Perdereau V, Adorno BV, Fraisse P. 2010. Position and orientation control of robot manipulators using dual quaternion feedback. In 2010 IEEE/RSJ International Conference on Intelligent Robots and Systems, pp. 658–63. Piscataway, NI: IEEE
- 57. Filipe N. 2014. Nonlinear pose control and estimation for space proximity operations: an approach based on dual quaternions. PhD Thesis, Ga. Inst. Technol., Atlanta, GA
- 58. Clifford WK. 1873. Preliminary sketch of bi-quaternions. Proc. Lond. Math. Soc. 4:381-95
- 59. Fischer IS. 2017. Dual-Number Methods in Kinematics, Statics and Dynamics. Boca Raton, FL: CRC
- Valverde A. 2018. Dynamic modeling and control of spacecraft robotic systems using dual quaternions. PhD Thesis, Ga. Inst. Technol., Atlanta, GA
- Valverde A, Tsiotras P. 2018. Dual quaternion framework for modeling of spacecraft-mounted multibody robotic systems. Front. Robot. AI 5:128
- Valverde A. 2018. Dynamic modeling and control of spacecraft robotic systems using dual quaternions. PhD Thesis, Ga. Inst. Technol., Atlanta, GA
- Filipe N, Tsiotras P. 2013. Simultaneous position and attitude control without linear and angular velocity feedback using dual quaternions. In 2013 American Control Conference (ACC), pp. 4808–13. Piscataway, NJ: IEEE

- Masutani Y, Miyazaki F, Arimoto S. 1989. Modeling and sensory feedback control for space manipulators.
 In Proceedings of the NASA Conference on Space Telerobotics, Vol. 3, pp. 287–96. Pasadena, CA: Jet Propuls.
 Lab.
- Dubowsky S, Papadopoulos E. 1993. The kinematics, dynamics, and control of free-flying and free-floating space robotic systems. IEEE Trans. Robot. Autom. 9:531–43
- Oda M. 1996. Coordinated control of spacecraft attitude and its manipulator. In Proceedings of the IEEE International Conference on Robotics and Automation (ICRA), Vol. 1, pp. 732–38. Piscataway, NJ: IEEE
- Senda K, Murotsu Y, Nagaoka H, Mitsuya A. 1995. Attitude control for free-flying space robot with CMG (Control Moment Gyroscopes). In *Guidance, Navigation, and Control Conference*, pp. 1494

 –502. Reston, VA: Am. Inst. Aeronaut. Astronaut.
- Giordano AM, Ott C, Albu-Schäffer A. 2019. Coordinated control of spacecraft's attitude and end-effector for space robots. IEEE Robot. Autom. Lett. 4:2108–15
- Oki T, Nakanishi H, Yoshida K. 2008. Time-optimal manipulator control of a free-floating space robot with constraint on reaction torque. In 2008 IEEE/RSJ International Conference on Intelligent Robots and Systems, pp. 2828–33. Piscataway, NJ: IEEE
- Parlaktuna O, Ozkan M. 2004. Adaptive control of free-floating space manipulators using dynamically equivalent manipulator model. *Robot. Auton. Syst.* 46:185–93
- Lampariello R, Agrawal S, Hirzinger G. 2003. Optimal motion planning for free-flying robots. In 2003 International Conference on Robotics and Automation (ICRA), Vol. 3, pp. 3029–35. Piscataway, NJ: IEEE
- 72. Jacobsen S, Zhu C. 2002. Planning of safe kinematic trajectories for free-flying robots approaching an uncontrolled spinning satellite. In Proceedings of the ASME 2002 International Design Engineering Technical Conferences and Computers and Information in Engineering Conference, Vol. 5: 27th Biennial Mechanisms and Robotics Conference, pp. 1145–51. New York: Am. Soc. Mech. Eng.
- Chen Y, Meirovitch L. 1995. Control of a flexible space robot executing a docking maneuver. J. Guid. Control Dyn. 18:756–66
- Grewal A, Modi V. 1995. Dynamics and control of flexible multibody systems: an application to orbiting
 platforms. In *IEEE International Conference on Systems, Man and Cybernetics: Intelligent Systems for the 21st Century*, Vol. 3, pp. 2093–98. Piscataway, NJ: IEEE
- Walker M, Wee LB. 1991. Adaptive control of space-based robot manipulators. IEEE Trans. Robot. Autom. 7:828–35
- 76. Ortega R, Spong MW. 1989. Adaptive motion control of rigid robots: a tutorial. Automatica 25:877-88
- 77. Slotine JJE, Li W. 1987. On the adaptive control of robot manipulators. Int. J. Robot. Res. 6:49-59
- Senda K, Nagoaka H, Murotsu Y. 1999. Adaptive control of free-flying space robot with position/attitude control system. J. Guid. Control Dyn. 22:488–90
- Masutani Y, Miyazaki F, Arimoto S. 1989. Sensory feedback control for space manipulators. In Proceedings
 of the 1989 International Conference on Robotics and Automation (ICRA), Vol. 3, pp. 1346–51. Piscataway, NJ:
 IEEE
- Caccavale F, Siciliano B. 2001. Quaternion-based kinematic control of redundant spacecraft/manipulator systems. In *Proceedings of the 2001 IEEE International Conference on Robotics and Automation (ICRA)*, pp. 435–40. Piscataway, NJ: IEEE
- 81. Nakamura Y, Mukherjee R. 1989. Nonholonomic path planning of space robots. In *Proceedings of the 1989 International Conference on Robotics and Automation (ICRA)*, pp. 1050–55. Piscataway, NJ: IEEE
- Nakamura Y, Mukherjee R. 1991. Nonholonomic path planning of space robots via a bidirectional approach. IEEE Trans. Robot. Autom. 7:500–14
- 83. Nanos K, Papadopoulos E. 2011. On the use of free-floating space robots in the presence of angular momentum. *Intell. Serv. Robot.* 4:3–15
- 84. Giordano AM, Garofalo G, De Stefano M, Ott C, Albu-Schäffer A. 2016. Dynamics and control of a free-floating space robot in presence of nonzero linear and angular momenta. In *IEEE 55th Conference on Decision and Control (CDC)*, pp. 7527–34. Piscataway, NJ: IEEE
- Papadopoulos E, Dubowsky S. 1991. On the nature of control algorithms for free-floating space manipulators. *IEEE Trans. Robot. Autom.* 7:750–58

- Nanos K, Papadopoulos E. 2012. On Cartesian motions with singularities avoidance for free-floating space robots. In 2012 IEEE International Conference on Robotics and Automation (ICRA), pp. 5398–403. Piscataway. NI: IEEE
- Nanos K, Papadopoulos E. 2015. Avoiding dynamic singularities in Cartesian motions of free-floating manipulators. *IEEE Trans. Aerosp. Electron. Syst.* 51:2305–18
- 88. Reyhanoglu M, McClamroch NH. 1991. Reorientation of space multibody systems maintaining zero angular momentum. In *Navigation and Control Conference*, pp. 1330–40. Reston, VA: Am. Soc. Mech. Eng.
- Reyhanoglu M, McClamroch NH. 1991. Controllability and stabilizability of planar multibody systems with angular momentum preserving control torques. In *Proceedings of the 1991 American Control Conference*, pp. 1102–107. Piscataway, NJ: IEEE
- 90. Nijmeijer H, van der Schaft A. 1990. Nonlinear Dynamical Control Systems. New York: Springer
- Nanos K, Papadopoulos E. 2017. On the dynamics and control of free-floating space manipulator systems in the presence of angular momentum. Front. Robot. AI 4:26
- Haddad WM, Chellaboina V. 2011. Nonlinear Dynamical Systems and Control: A Lyapunov-Based Approach. Princeton, NJ: Princeton University Press
- Filipe N, Valverde A, Tsiotras P. 2016. Pose tracking without linear and angular-velocity feedback using dual quaternions. IEEE Trans. Aerosp. Electron. Syst. 52:411–22
- Saleh JH, Castet JF. 2011. Spacecraft Reliability and Multi-State Failures: A Statistical Approach. Hoboken, NJ: Wiley & Sons
- 95. Polites ME. 1999. Technology of automated rendezvous and capture in space. 7. Spacecr. Rockets 36:280-91
- Natl. Aeronaut. Space Adm. 2020. 2020 NASA Technology Taxonomy. Washington, DC: Natl. Aeronaut. Space Adm. https://www.nasa.gov/sites/default/files/atoms/files/2020_nasa_technology_taxonomy.pdf
- 97. Dimitrov D. 2005. Dynamics and control of space manipulators during a satellite capturing operation. PhD Thesis, Tohoku Univ., Sendai, Jpn.
- Xu S, Wang H, Zhang D, Yang B. 2014. Extended Jacobian based adaptive zero reaction motion control for free-floating space manipulators. In *Proceedings of the 33rd Chinese Control Conference*, pp. 8359

 –64. Piscataway. NI: IEEE
- Dubanchet V, Saussié D, Alazard D, Bérard C, Le Peuvédic C. 2015. Modeling and control of a space robot for active debris removal. CEAS Space J. 7:203–18



Annual Review of Control, Robotics, and Autonomous Systems

Volume 6, 2023

Contents

An Overview of Soft Robotics Oncay Yasa, Yasunori Toshimitsu, Mike Y. Michelis, Lewis S. Jones, Miriam Filippi, Thomas Buchner, and Robert K. Katzschmann
Soft Actuators and Robots Enabled by Additive Manufacturing Dong Wang, Jinqiang Wang, Zequn Shen, Chengru Jiang, Jiang Zou, Le Dong, Nicholas X. Fang, and Guoying Gu
Adaptive Control and Intersections with Reinforcement Learning Anuradha M. Annaswamy
On the Timescales of Embodied Intelligence for Autonomous Adaptive Systems Fumiya Iida and Fabio Giardina
Toward a Theoretical Foundation of Policy Optimization for Learning Control Policies Bin Hu, Kaiqing Zhang, Na Li, Mehran Mesbahi, Maryam Fazel, and Tamer Başar
Sequential Monte Carlo: A Unified Review **Adrian G. Wills and Thomas B. Schön
Construction Robotics: From Automation to Collaboration Stefana Parascho
Embodied Communication: How Robots and People Communicate Through Physical Interaction Aleksandra Kalinowska, Patrick M. Pilarski, and Todd D. Murphey
The Many Facets of Information in Networked Estimation and Control Massimo Franceschetti, Mohammad Javad Khojasteh, and Moe Z. Win
Crowd Dynamics: Modeling and Control of Multiagent Systems Xiaoqian Gong, Michael Herty, Benedetto Piccoli, and Giuseppe Visconti
Noise in Biomolecular Systems: Modeling, Analysis, and Control Implications Corentin Briat and Mustafa Khammash

Exploiting Liquid Surface Tension in Microrobotics Antoine Barbot, Francisco Ortiz, Aude Bolopion, Michaël Gauthier,	
and Pierre Lambert	313
Spacecraft-Mounted Robotics Panagiotis Tsiotras, Matthew King-Smith, and Lorenzo Ticozzi	335
Grasp Learning: Models, Methods, and Performance *Robert Platt**	363
Control of Multicarrier Energy Systems from Buildings to Networks Roy S. Smith, Varsha Behrunani, and John Lygeros	391
Control of Low-Inertia Power Systems Florian Dörfler and Dominic Groß	415
How the CYBATHLON Competition Has Advanced Assistive Technologies Lukas Jaeger, Roberto de Souza Baptista, Chiara Basla, Patricia Capsi-Morales, Yong Kuk Kim, Shuro Nakajima, Cristina Piazza, Michael Sommerhalder, Luca Tonin, Giacomo Valle, Robert Riener, and Roland Sigrist	447
Into the Robotic Depths: Analysis and Insights from the DARPA Subterranean Challenge	
Timothy H. Chung, Viktor Orekhov, and Angela Maio	477

Errata

An online log of corrections to *Annual Review of Control, Robotics, and Autonomous Systems* articles may be found at http://www.annualreviews.org/errata/control